A Molecular Modeling Study on the Propagation in Free Radical Chain Oxidation of (B)PEI

Wim Buijs *

Posted Date: 28 January 2025

doi: 10.20944/preprints202501.2059.v1

Keywords: Density Functional Theory, Free Radical Chain Autoxidation, Basic Autoxidation Scheme, PEI

Article

A Molecular Modeling Study on the Propagation in Free Radical Chain Oxidation of (B)PEI

Wim Buijs *

Delft University of Technology

* Correspondence: wbuijsm@gmail.com

Abstract: Air oxidation of PEI is a Free Radical Chain Autoxidation process, described as a process following the Basic Autoxidation Scheme with Initiation, Propagation and Termination as discriminating steps. Molecular Modeling was able to identify the most important propagation reactions. HO_2•(d) is the most likely candidate as the main oxidation chain carrying radical. α-H-abstraction from PEI α-amino hydroperoxides by HO_2•(d) leading to amide PEI repeat units and eventually to HO_2•(d) again, is the first step in Propagation. Apart from well know propagation reactions, the reaction of PEI α-amino CH•(d) radicals with H_2O_2 is of major importance too with an estimated contribution of ~50% to Propagation. Furthermore it provides an explanation for the formation of NH_3 and various imine PEI repeat units. PEI α-amino alkoxy radicals might contribute to some extent to Propagation and can lead to chain breaks in PEI and the formation of CO_2. Amide and imine PEI repeat units contribute to ~90% in the fully oxidized PEI.

Keywords: density functional theory; free radical chain autoxidation; basic autoxidation scheme

1. Introduction

CO_2 capture is an important emerging technology to mitigate climate change [1,2]. Amine resins are intensively investigated as potential materials for CO_2 capture both from air and large point emission sources, like power plants and energy intensive industries [3-9]. They show good reversible CO_2 uptake and release however their long term oxidation stability might be a drawback for practical application [10-16]. This is particularly true for Direct Air Capture (DAC) of CO_2 which inherently deals with widely varying conditions with respect to temperature, humidity, contaminations, even within one day.

Among these resins PEI (Poly Ethylene Imine) is well known as a potential suitable material for CO_2 capture [5]. PEI is a collective name for a series of polymers with different molecular weights which can be divided in two main categories: LPEI (Linear Poly Ethylene Imine) and BPEI (Branched Poly Ethylene Imine). These differences do not only affect their structures (LPEI shows (a) crystal structure(s) and is (partly) solid till 50-110°C [17-22], while BPEI is usually a viscous liquid [23,24], but also their chemical (catalytic) reactivity not only in CO_2 capturing reactions but also in oxidative degradation. Parts of the oxidative degradation of organic polymers are not well understood due to the enormous variety of oxidation products and varying reaction rates. The simple repetitive structure of PEI could allow identification of all major oxidation products and reaction mechanisms. The identification of these products and reaction mechanisms transcends the importance for PEI and might contribute to the understanding of oxidative degradation of organic polymers in general.

With respect to air oxidation it is essential to realize that the most stable form of O_2 is *triplet* dioxygen, O_2(t), which means that despite its even number of electrons it has two *unpaired* electrons and thus behaves like a biradical. Most organic molecules are singlets which means that they have no unpaired electrons. To allow an organic molecule to react with O_2(t), either O_2(t) has to be converted to O_2(s), or the organic molecule RH(s) has to be converted to R•(d). The latter is the

 doi:10.20944/preprints202501.2059.v1

common process and leads directly to Free Radical Chain Autoxidation (FRCA) or Basic Autoxidation Scheme (BAS) [25,26]. FRCA is not limited to the oxidative degradation of polymers but is also observed in the air oxidation of bulk chemicals such cyclohexane [27-28].

In FRCA three major steps are identified: 1. Initiation, 2. Propagation, and 3. Termination.

1. Initiation

$RH + X \rightarrow R\bullet(d) + XH$

2. Propagation

$R\bullet(d) + O_2(t) \rightarrow RO_2\bullet(d)$

$RO_2\bullet(d) + RH \rightarrow RO_2H + R\bullet(d)$

3. Termination

$2\ RO_2\bullet(d) \rightarrow R{=}O + ROH + O_2(t)$

1. Initiation

If Initiation occurs with $O_2(t)$ itself, then it is the reaction step with the highest activation barrier thus determining the ultimate stability of a substrate against air oxidation. However, initiators, like transition metal complexes or peroxides, significantly lower that initiation activation barrier. In earlier publications [15,16] the importance of step 1. Initiation was extensively discussed including the role of transition metal complexes and other initiators.

2. Propagation

Propagation at least consists of two reactions to create the "chain" in FRCA. The first reaction:

1) $R\bullet(d) + O_2(t) \rightarrow RO_2\bullet(d)$

has no activation barrier at all while the activation barrier of the second reaction:

2) $RO_2\bullet(d) + RH \rightarrow RO_2H + R\bullet(d)$

will depend on the reactivity of both $RO_2\bullet(d)$ and RH. The reactivity of $RO_2\bullet(d)$ is considerably higher than the reactivity of $O_2(t)$. In most organic substrates several H-atoms can be abstracted and thus several $RO_2\bullet(d)$ species formed. In addition, the reactive $RO\bullet(d)$ can be formed from the self-reaction of two $RO_2\bullet(d)$ radicals which also can contribute to the chain:

3) $2\ RO_2\bullet(d) \rightarrow 2\ RO\bullet(d) + O_2(t)$

This reaction takes place via initial dimerization of the peroxyradicals to either a weak complex RO_2--O_2R or a highly reactive intermediate RO_4R [29,30] which decomposes almost barrier free to the products. Finally, the fate of the initially formed hydroperoxide (RO_2H) plays an important role in the propagation phase. In older literature [25,31] homolytic dissociation of RO_2H into $RO\bullet(d)$ + $OH\bullet(d)$ is a major reaction in the propagation as it produces two very reactive radicals which contribute strongly to the chain reaction.

As mentioned in the title the focus of this article is on step 2, Propagation in the FRCA of Poly Ethylene Imine (PEI). PEI is not only a relevant polymer for CO_2 capture, but its simple repetitive structure might enable the elucidation of the mechanisms of the formation of experimentally observed FRCA products by the application of Molecular Modeling.

3. Termination

For termination of the chain usually the coupling of two peroxyradicals ($RO_2\bullet(d)$) is chosen as they are more stable than the organic substrate radical ($R\bullet(d)$) and as a result they can build up to some extent. Another self-reaction of $RO_2\bullet(d)$ is often described as a termination reaction too [29,30]:

4) $2\ RO_2\bullet(d) \rightarrow R{=}O + ROH + O_2(t)$

Other termination reactions will be discussed as far they are of interest for the discussion on Propagation.

In this article new molecular modeling results obtained for PEI will be compared with:

1. Experimental work on PEI in the literature [10-14],
2. Molecular modeling results from the literature obtained for FRCA of cyclohexane [27,28], and

 doi:10.20944/preprints202501.2059.v1

3. Molecular modeling and chemical engineering modeling results for air oxidation of toluene [32,33].

2. Materials and Methods

Molecular Modeling calculations were conducted with Spartan '20 and '24 of Wavefunction [34]. This commercial package contains many methods, ranging from Molecular Mechanics, semi-empirical, Hartree-Fock to Density Functional Quantum Mechanical calculations, applying codes well described in the literature. In addition specific tasks are specified to ease the setup of calculations. For this article the tasks Conformer Distribution, Equilibrium Geometry, Energy Profile and Transition State Geometry were used frequently. Guesses for Transition State Geometries were quite often obtained via Energy Profiles wherein the distance between the presumed reaction centers stepwise was lowered until they are in chemical bonding reach. Finally, a wide variety of properties can be calculated, ranging from thermodynamic data to various spectra (NMR, UV, IR, Raman) which allows comparison with experimental data. Both thermodynamic data and IR-spectra were frequently used also.

A crucial step in Molecular Modeling is finding good starting structures for the calculations. While this is easy for small and rigid molecules, it turns out to be a tedious task for larger flexible molecules, like the oligomers of PEI. Molecular Mechanics is often the only possibility due to the extremely large numbers of conformers, the reliability of the method with respect both to structure and relative energy, and the apparent lack of experimental data on conformers and their distribution at equilibrium. The MMFF forcefield [35] was used to obtain Conformer Distributions, as to the best of my knowledge, this is the only forcefield wherein a comparison is made between computational results and scarce experimental data. An additional advantage of Molecular Mechanics is the explicit description of Van der Waals interactions.

The candidate structures of PEI oligomers obtained with MMFF were used as input for quantum chemical calculations (Equilibrium and Transition State Geometries) using density functional theory. Wherever possible MMFF structures were used as a guide to create even smaller models while still keeping essential elements of the original larger structures but for some transition state structures the semi-empirical PM3 was used as input for DFT calculations. This not only saves computational time but reduces the absolute error in DFT calculations also with respect to size and limited account of dispersive (Van der Waals) interactions. The latter is an intrinsic problem for most DFT codes because DFT calculations yield mean electron densities of molecular systems. Attempts to overcome this, for example that of Grimme [36] by reparameterization of DFT-codes, leading to DFT-D3 codes, are only partly successful and can cause other problems [37,38]. Therefore B3LYP/6-31G* was applied because it belongs to the most applied and validated codes and its merits and drawbacks are well known. The error in DFT calculations was further reduced by applying as much as possible the concept of isodesmic reactions [39], which leads to a cancellation of errors in estimates for the reaction enthalpy and activation enthalpy. Transition States were characterized by their unique imaginary frequency or internal reaction coordinate (IRC) [40]. Reaction energies and activation barriers were estimated from the sum of B3LYP/6-31G* total energies and enthalpy corrections. Entropy corrections were not applied due to the large simplifications of the models used for DFT calculations.

3. Results

3.1. Experimental Results from Literature

In close collaboration with Global Thermostat, Inc, a start-up in DAC-CO_2, Nezam et al., reported on the chemical kinetics of the oxidation of poly-ethylenimine in CO_2 sorbents [10]. Additionally important data can be found in Supporting Information in this article. In this study PEI-800 impregnated on γ-Al_2O_3 was used. PEI-800, a viscous liquid, is a BPEI oligomer with an average molecular weight of 800 g/mol according to LS and 600 g/mol according to GPC [23]. This corresponds to an average chain length of 18 (LS) or 14 (GPC) ethylenimine units with NH2-

 doi:10.20944/preprints202501.2059.v1

endgroups. They carried their oxidation study applying three different temperatures (125°C, 137.5°C and 150°C) and three different O_2 concentrations (5%, 17% and 21%) under dry conditions. The extent of oxidation was measured using two techniques: a) loss of amine efficiency to capture CO_2, and b) Differential Scanning Calorimetry (DSC). In addition, Thermogravimetric Analysis (TGA) and elemental analysis were conducted.

They showed that the two methods for the determination of the extent of oxidation perform consistently very well, albeit it that loss of amine efficiency is always faster than the heat production measured by DSC. The curves obtained with DSC in particular show a distinct s-shape. Loss of amine efficiency (total oxidation) was obtained in approximately 250 -1000 minutes with temperatures ranging from 150°C to 125°C. Under these circumstances total oxidation does not mean total combustion to volatile products like CO_2, H_2O and NH_3. Under the reaction conditions applied 82-87% of the mass of BPEI was retained at 5-30% of O_2, relatively unaffected by temperature. The latter is a clear sign that not only mass was removed by evaporation of volatile oxidation products but also oxygen was incorporated in the polymer backbone. Furthermore, the normalized C/N ratio increases from1.0 to 1.2 from start to total oxidation, while the normalized H/(C+N) ratio decreases from 1.0 to 0.7. This accounts for a loss of ~20% of the amine groups, converted either to NH_3 or other volatile N-containing products. The loss of hydrogen can be explained by the formation of H_2O.

The activation barrier was measured as a function of the extent of oxidation. After a short induction period, an average activation barrier of ~105 kJ/mol ± 10 kJ/mol was obtained in the oxidation range from 10-70%. Beyond 70% oxidation the activation barrier drops rapidly to < 30 kJ/mol at almost total oxidation.

The reaction order in O_2 was found to be between 0.5 (125°C) and 0.7 (150°C) up to ~50% extent of oxidation whereafter it drops to almost 0.

As a direct continuation of the experimental research described above, in a research collaboration between Global Thermostat and the Livermore National Laboratory, Racicot et al., described the formation of volatile products from the autoxidation of (B)Pei-800 [11]. It was found that NH_3, H_2O and CO_2 were produced in a rather constant ratio during the autoxidation process. At the end of the autoxidation process the ratio of NH_3/N-BPEI ~ 0.21, H_2O/H-PEI ~ 0.10 and CO_2/C-PEI ~ 0.02.

Apart from experimental results, some computational results were presented too. An attempt to account for the formation of NH_3, using Tri-Ethylene-Tetra-Amine (TETA) as a small model for BPEI and applying a metadynamics approach, yielded a ΔG_{act} = 282 kJ/mol for the direct elimination of NH_3 from TETA, while a process starting from the TETA β-radical yielded NH_2(d) and the corresponding N-vinyl-Di-Ethylene-Tri-Amine (N-vinyl-DETA) with a ΔG_{act} ~ 90 kJ/mol. The reaction of NH_2(d) with N-vinyl-DETA or an additional TETA yields NH_3 and another radical in an essentially barrier free process. This radical process fits with the experimental mean activation barrier of ~105 kJ/mol during the propagation phase of the autoxidation as discussed above. No attempts were made to relate computational results with the quantitative observed amounts of all volatile products, NH_3, H_2O and CO_2.

Ahmadalinezhad and Sayari [13] studied oxidative degradation of PEI impregnated on mesoporous silica at various temperatures. They used solvent extraction to remove the oxidated PEI from the mesoporous silica and applied a variety of NMR techniques to identify structural elements in the oxidated PEI. It is important to note that they studied both BPEI and LPEI. They found that both oxidized LPEI and BPEI contained $RNHCH_2$-C=O-NHR* and RNH-CH_2-CH=NR* units but RNH-C=O-CH=NR* units were observed in oxidized BPEI only.

Min et al., observed in their work on the oxidation stability of BPEI [14,24] on a silica support a sharp increase in an IR-adsorption at 1670 cm^{-1}, related to the formation of C=O and/or C=N bonds, and a decrease in IR-adsorptions between 2800-3000 cm^{-1}, related to the disappearance of C-H bonds in oxidized BPEI. The C=O and/or C=N bonds were attributed to the formation of amides and imines in line with the findings of Ahmadalinezhad and Sayari [13].

 doi:10.20944/preprints202501.2059.v1

3.2. Computational Results from Literature

The oxidation of cyclohexane is an important industrial process with an annual production of ~10^6 tons/year. Its product is the so-called **KA**-oil which consists of cyclohexanone (**K**etone) and cyclohexanol (**A**lcohol). Cyclohexanol is converted in a separated catalytic process to cyclohexanone too. Next cyclohexanone is converted to caprolactam, the feedstock for nylon-6. The oxidation of cyclohexane with air is carried out at ~160°C at a low conversion, at the cost of a relatively high energy consumption, to keep the selectivity to cyclohexanone and cyclohexanol high enough to be economically feasible. At higher conversion of cyclohexane both the amount and number of side products increase so fast that the process is no longer attractive. The reaction proceeds via an FRCA-mechanism. In the propagation step a cyclohexyl radical (Cy •(d)) reacts with O_2(t) to yield the cyclohexylperoxy radical (CyOO•(d). In the next step the cyclohexylperoxy radical abstracts a H-atom from cyclohexane (CyH) to yield cyclohexyl hydroperoxide (CyOOH) and a new cyclohexyl radical, as described as reaction 1 and 2 in the introduction:

5) Cy•(d) + O_2(t) → CyO_2•(d)

6) CyO_2•(d) + CyH → CyO_2H + Cy•(d)

The decomposition of CyO_2H into CyO•(d) and HO•(d) is thought to contribute to the propagation as the HO•(d) radical will abstract a H-atom from CyH to yield Cy•(d) and H_2O. Product formation to cyclohexanone (Cy=O) and cyclohexanol (CyOH) is considered as a termination step from the reaction of two CyO_2•(d) radicals as described as reaction 4 in the introduction too:

7) 2 CyO_2•(d) → Cy=O + CyOH + O_2(t)

Hermans et al., [27] experimentally observed the rapid formation of CyO_2H, Cy=O and CyOH as a function of conversion at 145°C and suggested that product formation, to Cy=O and CyOH, must originate from fast propagation steps. They applied DFT calculations to identify the mechanism behind the observed formation of the products. They found that the activation barriers for α-H-atom abstraction from CyO_2H and CyOH by CyO_2•(d) are ~24 and 22 kJ/mol respectively lower than from CyH and the corresponding reaction rate 20-80 and 5-20 faster, taking into account the relative number of H-atoms that can be abstracted in both cases. The lowering of the activation barrier for a-H-atom abstraction from Cy=O by CyO_2•(d) is only 8 kJ/mol lower. Thus, propagation in FRCA starting from CyO_2H and CyO_2•(d) is an important channel for propagation. The formal initial product of that reaction, the α-Cy•(OOH)(d) radical, decomposes directly into Cy=O and HO•(d) which contributes to the propagation also.

8) CyO_2H + CyO_2•(d) → CyO_2H + α-Cy•(OOH)(d)

α-Cy•(OOH)(d) → Cy=O + HO•(d)

The formation of CyOH was explained by another propagation step instead of a termination step:

9) CyO_2•(d) + CyH → CyO_2H + Cy•(d)

10) CyO_2H + Cy•(d) → CyOH + HO•(d)

The first step is a normal propagation step rate as described in reaction 6. However in the cyclohexane bulk liquid phase the rate of the second step, reaction 10, would be 4-5 orders of magnitude lower than reaction 9, and thus not likely. The assumption that initially the reaction takes place in a so called "Franck–Rabinowitch" solvent cage [40] leads to an estimated reaction rate which much better coincides with the observed rate but still is slightly too slow. At higher conversion a major role in the propagation process is taken by HO•(d) which leads to the formation of CyO•(d). The CyO•(d) radical yields ~60-70% CyOH by H-atom abstraction and 40-30% ring-opening β-C-C cleavage products. They concluded that the formation of both Cy=O + CyOH can be much better explained by propagation reactions in the FRCA of cyclohexane. Though not highlighted as such, it is also clear that most of the byproducts in cyclohexane oxidation do not originate from cyclohexanone but instead originate from the CyO•(d) radical. In a study that can be considered as a continuation of the former study, Hermans et al., [28] addressed the experimental finding that cyclohexanone, amongst other ketones, clearly enhance the cyclohexane oxidation rate in the early stage of the oxidation. They propose an alternative reaction of CyO_2H with Cy=O and CyH:

 doi:10.20944/preprints202501.2059.v1

11) $CyO_2H + Cy{=}O \rightarrow CyO\bullet(d) + H_2O + Cy{=}O\ \alpha\text{-}CH\bullet(d)$ and

12) $CyO_2H + CyH \rightarrow CyO\bullet(d) + H_2O + Cy\bullet(d)$

This type of reaction requires a lower activation barrier of homolytic dissociation of CyO_2H into $CyO\bullet(d) + HO\bullet(d)$ which is about 170 kJ/mol. The authors were able to locate a Transition State with an activation barrier of ~100 kJ/mol. The difference between reactions 11 and 12 on one side, and reaction 10 on the other side is that in reaction 10, a hydrocarbon radical reacts with the hydroperoxide to yield an alcohol and an alkoxy radical, while in reactions 11 and 12, the hydroperoxide has to dissociate almost completely into an RO•(d) and an HO•(d) radical, whereafter the HO•(d) radical abstracts a H-atom to yield an RO•(d) radical, H_2O and an R•(d) radical. It can be considered as a modification of the old mechanism wherein homolytic dissociation of ROOH into RO•(d) and HO•(d) is a crucial step in the propagation [25,31].

3.3. Molecular Modeling and Chemical Engineering Modeling Results for Air Oxidation Of Toluene

Air oxidation of toluene is a FRCA process like air oxidation of cyclohexane and Hermans et al., [32] have published a study on the air oxidation of toluene also. Basic aspects of FRCA, as discussed above for cyclohexane oxidation, remain the same. An important result on top of that is that the $HO_2\bullet(d)$ radical gradually replaces the role of the benzylperoxy radical as chain carrying radical in the propagation. In 2005 a study appeared from Hoorn et al., [33] on the incorporation of mass transfer phenomena in the air oxidation of toluene. At that time DSM operated the largest toluene oxidation plant in the world, producing benzaldehyde, benzoic acid and sodium benzoate as fine chemicals. Excess of benzoic acid was converted into phenol in a separate Cu(I)/Cu(II) catalyzed oxidation step. The overall process is known as the DOW-Phenol process [42]. Nowadays Noveon Kalama Inc. [43] operates this process. The study of Hoorn et al., [33] is of interest for propagation in FRCA of PEI because it addresses mass transfer phenomena which is often neglected in kinetic studies. Based on an in-depth chemical engineering analysis of the experimentally observed reaction rate and the mass transfer rate of O_2 it was concluded that under industrial conditions (T= 140-160°C, P= 4-7 bar) the overall toluene oxidation rate is slow in comparison to the mass transfer rate of oxygen.

4. Computational Results

4.1. Model Systems

As described above the experimental work of Nezam et al., used BPEI with an average molecular weight of 800 g/mol and a corresponding average chain length of 18 [10,23]. Min et al. used a BPEI with an average molecular weight of 1200 g/mol and a corresponding average chain length of 27 [14,24]. Figure 1 shows a model for both types of BPEI.

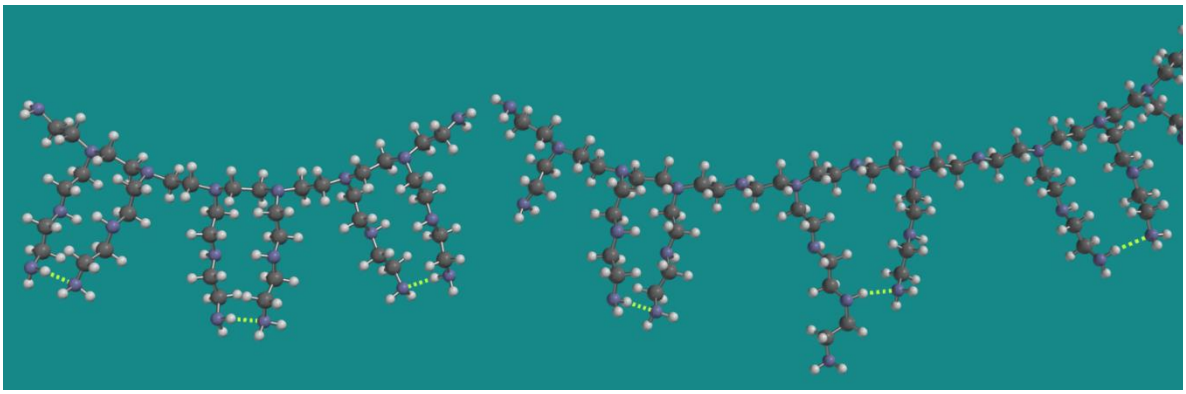

(**a**) (**b**)

Figure 1. MMFF BPEI models for a: PEI-800 Sigma-Aldrich PN 408719 [23] and b: Epomin SP-012 [24]; display: ball and spoke, C: grey, N: blue, H: white, hydrogen bridges: yellow.

 doi:10.20944/preprints202501.2059.v1

The models were constructed as described in detail previously by Buijs [15]. The molecular weight of the model for PEI-800 is 834 g/mol, corresponding to a chain length of 19. The amine composition is primary/secondary/tertiary = p/s/t = 8/6/6 or 40%/30%/30%. The molecular weight of the model for Epomin SP-012 is 1179 g/mol, corresponding to a chain length of 27. The amine composition is primary/secondary/tertiary = p/s/t = 10/10/8 or 36%/36%/28%, close to the analytical result of Min et al. [14]. An important aspect of the MMFF models for BPEI is their CO_2 capacity, not only for material efficiency reasons but also to determine the amount of oxidation as described above. Under dry conditions two amine groups are required to capture one CO_2 molecule [44,45]. The maximum CO_2 capacity of the model for PEI-800 is 3.6 mmol CO_2/g PEI-800 in line with the experimental observation of Nezam et al. [23]. With respect to that property the display of the model for Epomin SP-012 is a bit misleading as it suggests that in this case a similar amount of CO_2 can be captured, corresponding to 2.5 mmol CO_2/g Epomin SP-012. However the important characteristic of the model are the chain lengths, counted from the tertiary N-atoms. They should be at least two units long to allow two amines to come close enough to capture CO_2. This could be two primary amines, but a combination of a secondary and a primary amine is also possible. Furthermore, the distance between the tertiary N-atoms can be one or two units. The total number of possible energetically favorable amine-amine interactions is then five. This leads to 4.2 mmol CO_2/g Epomin SP-012 which is close to the value experimentally observed by Min et al. [14] of 4.0 mmol CO_2/g Epomin SP-012. Of course, various permutations on this structure can be made with a similar outcome.

The MMFF structures of BPEI were used were as input for quantum chemical calculations using B3LYP/6-31G* as described in 2. Materials and Methods. A common structural element in both models is the one where the tertiary N-atoms are separated by one unit only and the chain lengths of the units on the tertiary N-atoms is two. Therefore the earlier applied and smaller model N,N-3,4-dimethyl N6-pentamer of PEI was applied. As a control a full Conformer Distribution on this smaller model was determined, using MMFF. The total numbers of formal conformers for this small model is already > $2.29*10^8$. An energy threshold for conformers ≤ 20 kJ/mol above the strain energy of the best conformer was added to ease the analysis of computational results. The best conformer (MMFF) is shown in Figure 2, together with its non-amine H-bridged counterpart, both as MMFF and B3LYP/6-31G* geometry optimized structures. In addition, the numbering of the 6 N-atoms and the α,β numbering of the CH_2 groups is provided under b).

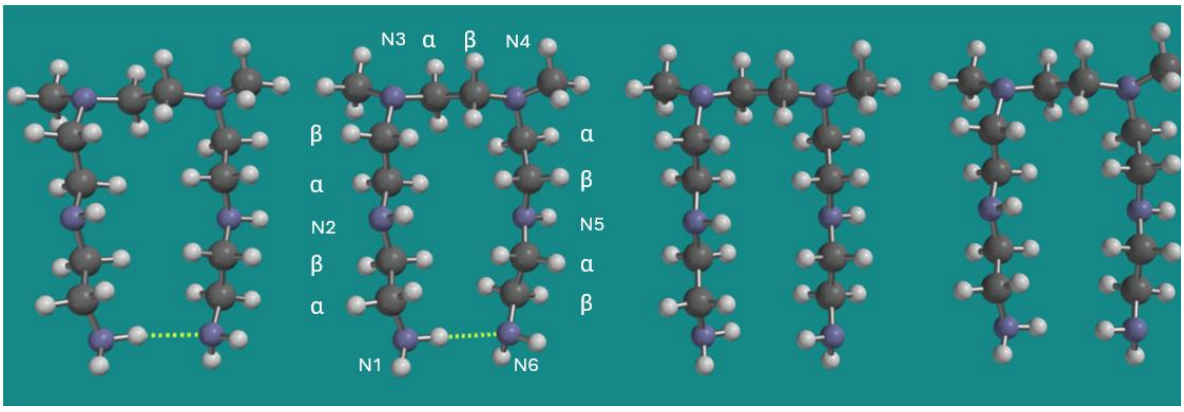

(**a**) (**b**) (**c**) (**d**)

Figure 2. N,N-3,4-dimethyl N6 pentamer as a small BPEI model for PEI-800 Sigma-Aldrich PN 408719 [23] and Epomin SP-012 [24]; a: H-bridged, MMFF, b: H-bridged, B3LYP/6-31G*, c: non H-bridged, MMFF, d: non-H-bridged, B3LYP/6-31G*. Display: ball and spoke, C: grey, N: blue, H: white, hydrogen bridges: yellow.

Visually structures a) and b) on one side, and c) and d) on the other side are very similar. The largest difference is the length of the RNH_2 – NH_2R H-bridge which is 2.198 Å for the MMFF structure and 2.324 Å for the B3LYP/6-31G* structure. Furthermore, the energy difference between the H-bridged and the non-H-bridged structures is 9.1 kJ/mol for the MMFF structure and 9.9 kJ/mol for the B3LYP/6-31G* structure in both cases in favor of the H-bridged structures. So, even though DFT

 doi:10.20944/preprints202501.2059.v1

methods like B3LYP are known to underestimate dispersive interactions, there is no serious discrepancy between the results obtained with MMFF and B3LYP/6-31G* in this particular case as relatively strong average electrostatic interactions are dominant.

As described by Buijs [15] H-atom abstraction by $O_2(t)$ is the rate determining step in the initiation of FCRA of PEI (reaction 13). Either the reaction of the α-amino CH•R-radical with $O_2(t)$ followed by reaction with the $HO_2•(d)$ radical (reaction 14 and 15) or the direct reaction with the $HO_2•(d)$ radical (reaction 16) yields the α-amino hydroperoxide. The latter reaction requires formally an intersystem crossing [46] as the two doublets originate from $O_2(t)$.

13) $R_2NCH_2CH_2NR_2 + O_2(t) \rightarrow R_2NCH•CH_2NR_2(d) + HO_2•(d)$

14) $R_2NCH•CH_2NR_2(d) + O_2(t) \rightarrow R_2NCHO_2•CH_2NR_2(d)$

15) $R_2NCHO_2•CH_2NR_2(d) + HO_2•(d) \rightarrow R_2NCH(O_2H)CH_2NR_2 + O_2(t)$ or

16) $R_2NCH•CH_2NR_2(d) + HO_2•(d) \rightarrow R_2NCH(O_2H)CH_2NR_2$

Both reaction pathways are possible because the initial H-atom abstraction is slow and at least during initiation there will be sufficient $O_2(t)$ while the $HO_2•(d)$ radical is relatively stable and might build up to a certain level.

4.2. Loss of Amine Efficiency

One of the observations of Nezam et al., [10] was that during the progress of FRCA of BPEI the loss of amine efficiency is always faster than the reaction heat production as indicated by DSC measurements. An attractive explanation for that observation comes from the results from Molecular Modeling on the relative stability of the conformers of various α-amino hydroperoxides. Figure 3 shows various MMFF N,N-3,4-dimethyl N6 pentamer α-amino hydroperoxides. The formation of an α-amino hydroperoxide in most cases causes a substantial change in the conformation of the original N,N-3,4-dimethyl N6 pentamer, leading to geometries where the two amino groups, which are required to capture CO_2, no longer are in each other vicinity. Though in the case of an α-amino hydroperoxide from a primary amine, an amine-amine H-bridge still seems possible as can be seen in Figure 3a, the hydroperoxide-amine H-bridge shown in Figure 3b, is 19.4 kJ/mol favorable than the amine-amine H-bridge shown in Figure 3a. In case of an α-amino hydroperoxide from a secondary amine, amine-amine H-bridges are no longer possible, neither in c) nor in d). The α-amino hydroperoxide c) is 34.0 kJ/mol higher in strain energy than b) while α-amino hydroperoxide d) is 61.3 kJ/mol higher in strain energy than b). Thus, already during the initial stage of the FRCA of BPEI loss of amine efficiency can be expected.

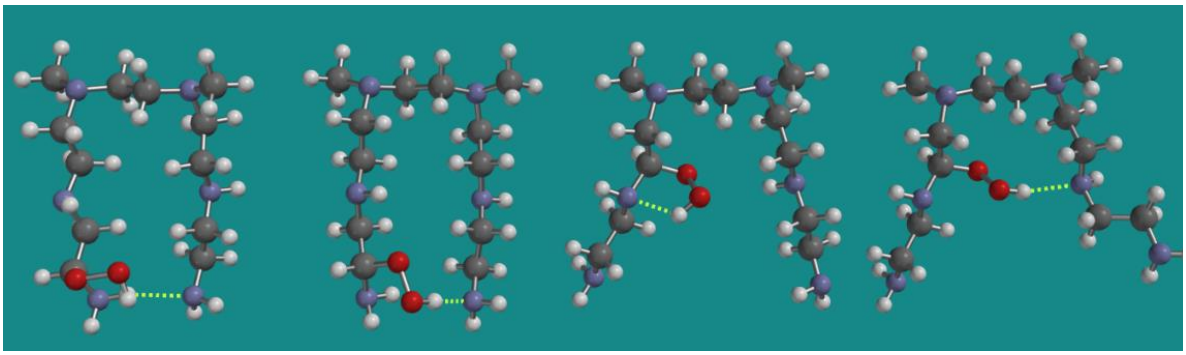

(**a**) (**b**) (**c**) (**d**)

Figure 3. Various MMFF N,N-3,4-dimethyl N6 pentamer amino hydroperoxides; a: N1-α-amino hydroperoxide NH-N H-bridged, b: N1-α-amino hydroperoxide ROOH-N H-bridged, c: N2-α-amino hydroperoxide intra-chain ROOH-N H-bridged, d: N2-α-amino hydroperoxide inter-chain ROOH-N H-bridged. Display: ball and spoke, C: grey, N: blue, H: white, hydrogen bridges: yellow.

 doi:10.20944/preprints202501.2059.v1

4.3. FRCA of PEI: Propagation

4.3.1. Decomposition of α-Amino Hydroperoxides by HO_2•(d) and HO•(d)

Decomposition of the α-amino hydroperoxide by a radical is the first step in the propagation. Several options are available and will be discussed:

17. $R_2NCH(O_2H)CH_2NR_2 + R_2NCHO_2•CH_2NR_2(d) \rightarrow R_2NC=OCH_2NR_2 + R_2NCH(O_2H)CH_2NR_2 + HO•(d)$

18. $R_2NCH(O_2H)CH_2NR_2 + HO_2•(d) \rightarrow R_2NC=OCH_2NR_2 + H_2O_2 + HO•(d)$

19. $R_2NCH(O_2H)CH_2NR_2 + HO•(d) \rightarrow R_2NC=OCH_2NR_2 + H_2O + HO•(d)$

Reaction 17 is the analogue of reaction 8 discussed by Hermans et al. [28]. With respect to the reactivity of α-amino hydroperoxyl radical, in principle the reaction should be as plausible as in cyclohexane oxidation. However the diffusion coefficient of the BPEI oligomer, PEI-800, is too low. Applying the classical relation of Wilke and Chang [47] and using the molecular volumes of the PEI-800 model and HO_2•(d) from their MMFF structures, it can be estimated that the diffusion coefficient of PEI-800 will be ~ 8* smaller than the diffusion coefficient of HO_2•(d). Thus, for BPEI this reaction is not likely to occur. In addition, the same reaction inside an oligomer, between two chains in close vicinity of each other, seems not plausible also because of steric hindrance as can be seen in Figure 3.

Therefore reaction 18 seems much more likely as the HO_2•(d) radical is mobile, relatively stable, and can build up to some extent. Thus, the HO_2•(d) radical might diffuse to other PEI-800 oligomers and make a large contribution to the FRCA chain length. H_2O_2 itself might contribute to the propagation chain by reaction with HO•(d) to yield H_2O and HO_2•(d) though it decomposes in H_2O and O_2(t) too.

Reaction 19 could be considered as the direct counterpart of reaction 17 in the propagation. However, the HO•(d) radical is extremely reactive and could easily abstract a variety of H-atoms available, including the H-atoms of H_2O_2 and HO_2•(d), in essentially barrier free reactions. Because of its high reactivity, its reactions might be limited to a single PEI-800 oligomer.

Table 1 provides an overview of all propagation reactions investigated, starting from reactions of various hydroperoxides with either HO_2•(d) or HO•(d), reactions starting from the N,N-3,4-dimethyl N6 pentamer with either N1-α-amino peroxy (d) or HO_2•(d) and reactions from H_2O_2 with α-amino radicals of the N,N-3,4-dimethyl N6 pentamer. Reactions of α-amino radicals with O_2(t) to yield α-amino hydroperoxyl radicals are barrier free and are not listed.

Table 1. Overview B3LYP/6-31G* activation barriers of propagation reactions with various N,N-3,4-dimethyl N6 pentamers and their α-amino hydroperoxides.

Entry	N,N-3,4-dimethyl N6 pentamer and R•(d)		E_a (kJ/mol)	n (cm^{-1})
1	N1-a-amino hydroperoxide	HO_2•(d)	115.7	i1790
2	N2-a-amino hydroperoxide	HO_2•(d)	93.9	i1486
3	N2-b-amino hydroperoxide	HO_2•(d)	112.3	i1597
4	N5-a-amino hydroperoxide	HO_2•(d)	85.5	i1265
5	N1-amide-b-hydroperoxide	HO_2•(d)	90.3	i1401
6	N1,2-diamide-N1-b-hydroperoxide	HO_2•(d)	103.9	i1639
7	N1-a-amino hydroperoxide	HO•(d)	21.2	i794
8	N2-b-amino hydroperoxide	HO•(d)	9.3	i989
9	N4-b-amino hydroperoxide	HO•(d)	9.9	i131
10	N5-a-H	N1-a-amino peroxy radical (d)	71.3	i1232
11	N3-a-H	N2-a-amino peroxy radical (d)	32.4	i1503
12	N4-b-H	N2-a-amino peroxy radical (d)	36.2	i1571

 doi:10.20944/preprints202501.2059.v1

13	N3-b-H	N2-b-amino peroxy radical (d)	71.2	i1370
14	N4-b-H	N5-a-amino peroxy radical (d)	80.2	i1568
15	N1-a-H	HO_2•(d)	92.9	i1507
16	N1-b-H	HO_2•(d)	84.3	i1375
17	N2-b-H	HO_2•(d)	107.0	i1510
18	N3-b-H	HO_2•(d)	85.1	i1524
19	N1-amide	HO_2•(d)	70.6	i1223
20	N2-amide	HO_2•(d)	100.0	i1668
21	N3-amide	HO_2•(d)	83.1	i1643
22	N1,N2-diamide	HO_2•(d)	85.8	i1751

The order for decomposition of the α-amino hydroperoxides with HO_2•(d) only partly reflects the order for H-abstraction from α-CH_2 groups of simple primary, secondary and tertiary amines [16] which sets a lower limit on the use of small model systems. For primary and tertiary amines (entries 1,3) the order coincides but for secondary amines (entries 2,4) the order is dominated by the steric hindrance between the chains of the starting α-amino hydroperoxides of the N,N-3,4-dimethyl N6 pentamer, resulting in higher energies of the starting complexes which are not reflected in the transition states. This leads to lower activation barriers of 93.9 and 85.5 kJ/mol for entries 2 and 4 respectively. Decomposition of α-amino hydroperoxides leads to the formation of the corresponding amides and the HO•(d) radical. The latter is usually converted to H_2O via a consecutive H-atom abstraction from either HO_2•(d), or H_2O_2, or a CH_2-group inside the N,N-3,4-dimethyl N6 pentamer and contributes to propagation too. The amide still contains an oxidizable CH_2-group, and entries 5 and 6 show the activation barriers for a mono-amide- and a diamide-hydroperoxide with values of 90.3 and 103.9 kJ/mol, respectively. As the electron density on the remaining CH-group of the hydroperoxides decreases, the activation barrier for H-abstraction by HO_2•(d) increases but stays well below the activation barrier for initiation.

Formation of amides increases the mass of the original PEI-800 oligomer, while lowering the H/(C+N) ratio in line with the experimental findings of Nezam et al., [10]. Figure 4 shows the decomposition of the N2-β-amino hydroperoxide with HO_2•(d) (entry 3) to the corresponding amide in three steps: a) the starting complex, b) the transition state and c) the product complex. All three structures show an H-bridge between HO_2•(d) and the secondary amine on the N2-position. In the transition state the C-H distance of the N2-β-amino hydroperoxide is 1.423 Å and the HOO-H distance is 1.141 Å. The product complex consists of the flat dialkyl amide, H_2O_2, and the HO•(d) radical. The HO•(d) radical is stabilized by two H-bridges, one to the amide-carbonyl oxygen and one to H_2O_2. This will lead also to the formation of HO_2•(d) and H_2O, as described above because H_2O_2 and HO•(d) are in close vicinity, thus limiting its role in the propagation as chain carrier radical. Furthermore, in case of the amide-hydroperoxides, HO_2•(d) preferably shows H-bridges to the carbonyl of the amides.

Finally, formation of the amide is strongly exothermic with an estimate for ΔH of -180.2 kJ/mol, in line with the results of the DSC-experiments of Nezam et al., [10] and the NMR results of Ahmadalinezhad et al., [13] identifying $R_2NCH_2C{=}O\text{-}NR_2$ as a structural element in the air oxidation of PEI.

 doi:10.20944/preprints202501.2059.v1

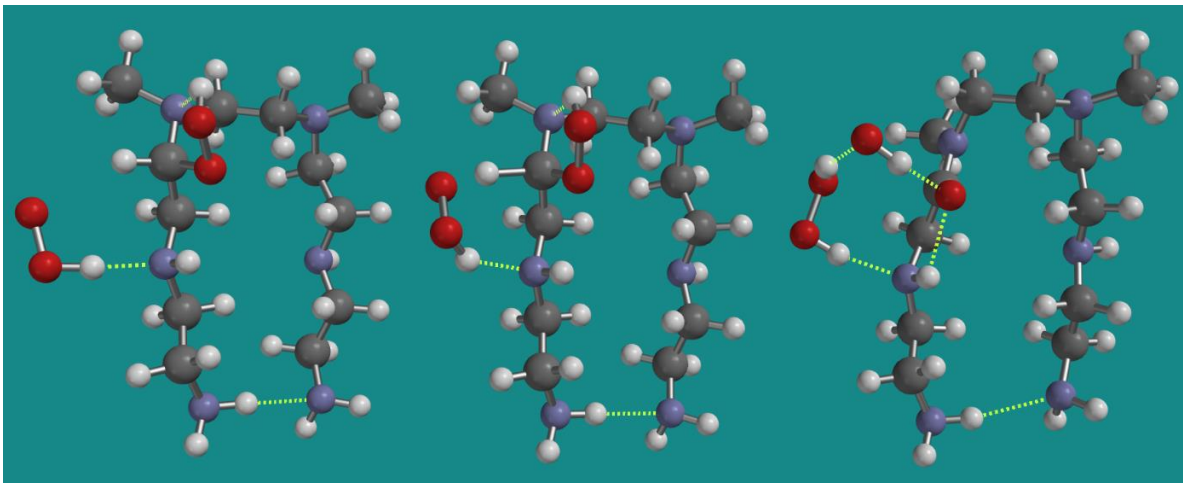

ν = i1597 cm^{-1}

(**a**) (**b**) (**c**)

Figure 4. Decomposition N2-β-amino hydroperoxide of N,N-3,4-dimethyl N6 pentamer with HO_2•(d); B3LYP/6-31G*, a: starting complex, b: transition state with its unique imaginary frequency, c: product complex. Display: ball and spoke, C: grey, N: blue, H: white, hydrogen bridges: yellow.

Decomposition of α-amino hydroperoxides by the HO•(d) radical, shown in entries 7-9, leads to the formation of amides too, H_2O and the HO•(d) radical. The activation barriers are much lower than in the case of HO_2•(d) and range from 9.3 to 21.2 kJ/mol only.

4.3.2. Propagation with α- and β-Amino Peroxy Radicals

Peroxy radicals contribute to the propagation chain. Figure 5 shows an overview of 5 transition states of the reaction of α- and β-amino peroxy radicals inside the PEI-800 model, the N,N-3,4-dimethyl N6 pentamer, as listed in Table 1, entries 10-14.

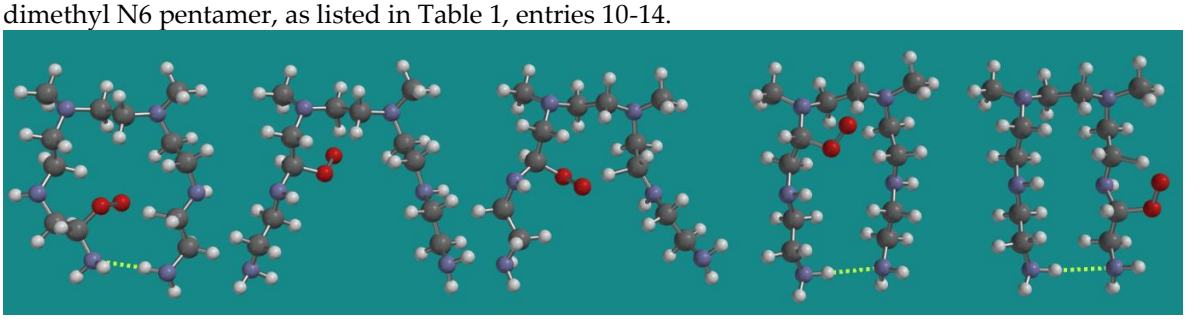

ν= i1232 cm^{-1} ν= i1503 cm^{-1} ν= i1571 cm^{-1} ν= i1370 cm^{-1} ν= i1568 cm^{-1}

N1-α-amino peroxy (d) N2-α-amino peroxy(d) N2-α-amino peroxy (d) N2-β-amino peroxy (d) N5-α-amino poxy (d).

to N5-α-H to N3-α-H to N4-β-H to N3-β-H to N4-β-H.

Figure 5. Propagation with α-amino peroxy radicals of the N,N-3,4-dimethyl N6 pentamer; B3LYP/6-31G*. Display: ball and spoke, C: grey, N: blue, H: white, hydrogen bridges: yellow.

The results show a clear division between entries 10, 13, and 14, and entries 11 and 12. Entries 10,13 and 14 show an activation barrier for internal H-abstraction of 71.3, 71.2 and 80.2 kJ/mol respectively, while entries 11 and 12 show activation barriers of 32.4 and 36.4 kJ/mol only. The latter is due to the steric hindrance in the starting structures and the corresponding higher energy of these peroxy radicals of ~40 kJ/mol. Even in the absence of steric hindrance the activation barriers are generally lower than the activation barriers for decomposition of the α-amino hydroperoxides by the HO_2•(d) radical. These propagation reactions intrinsically are limited to occur within one PEI-800 oligomer.

 doi:10.20944/preprints202501.2059.v1

4.3.3. Propagation with HO_2•(d) radical

The propagation reaction of various N,N-3,4-dimethyl N6 pentamers and their analogues amides with HO_2•(d) were investigated too. This is important as the propagation reactions investigated thus far almost exclusively take place in a single PEI-800 oligomer. The HO_2•(d) radical should be mobile, stable and reactive enough to be able to diffuse from one PEI-800 oligomer to another and abstract H-atoms from a variety of sources. Entries 16-19 list the results of the reactions of N,N-3,4-dimethyl N6 pentamers themselves with HO_2•(d). The activation barriers range from 84.1 for H-abstraction from N1-β-H to 107.0 kJ/mol for H-abstraction from N2-β-H. The relatively high activation barrier of this case is due to steric hindrance around the tertiary N3 in the transition state. All starting complexes show total energies ≤2 kJ/mol different from each other. In all cases the HO_2•(d) radical shows a strong H-bridge to either a secondary or a tertiary N-atom in the N,N-3,4-dimethyl N6 pentamer, very similar as shown and discussed in Figure 4a, the starting complex.

Entries 19-21 list the results of the reactions of various mono-amides derived from the original N,N-3,4-dimethyl N6 pentamer with HO_2•(d) and finally entry 22 shows the result for the corresponding N1,N2 di-amide derived from the original N,N-3,4-dimethyl N6 pentamer. Amides are not only the principal products of the radical decomposition of α-amino hydroperoxides but should be considered as substrates also, as they still contain oxidizable CH_2-groups. Figure 6 shows a typical example with the starting structure and the transition state of entry 22, H-abstraction by HO_2•(d) from the remaining CH_2-group of the N1,N2-diamide of the N,N-3,4-dimethyl N6 pentamer.

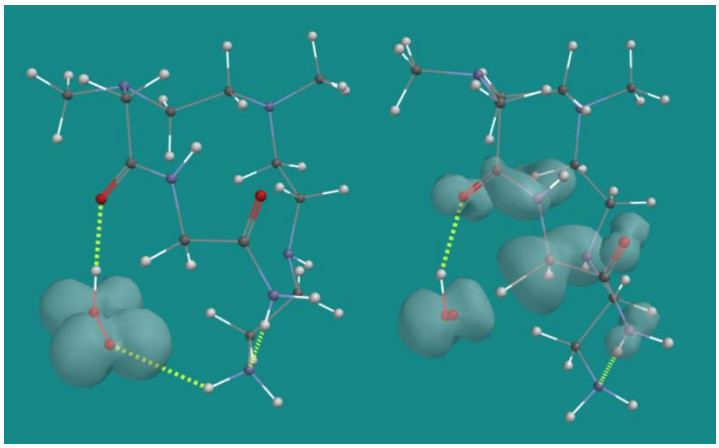

ν = i1751 cm^{-1}

(**a**) (**b**)

Figure 6. H-abstraction by HO_2•(d) from N1,N2-diamide of N,N-3,4-dimethyl N6 pentamer; B3LYP/6-31G*. a: starting complex, b: transition state; Display: ball and wire, C: grey, N: blue, H: white, hydrogen bridges: yellow; surface: spin density at isosurface =0.002 e/au^3.

The starting structure shows a H-bridge of HO_2•(d) to the amide carbonyl oxygen. The OOH-O=C distance is 1.686 Å. There are also weak H-bridges between the primary amine and the oxygen of HO_2•(d) with a distance of 2.433 Å and between the N1 amide-NH_2 and the N6 primary amine with a distance of 1.993 Å. In the transition state the H-bridges of HO_2•(d) to the amide carbonyl oxygen and the H-bridge between the N1 amide-NH_2 and the N6 primary amine are maintained with distances of 1.882 Å and 1.997 Å respectively. The C-H distance of the CH_2-group between the two amides is 1.360 Å and the OO-H distance is 1.195 Å. The spin density is extended to both amide groups, indicating considerable stabilization. The activation barrier for the diamide substrate is 85.8 kJ/mol, which is in the range of 70.6-100.0 kJ/mol for all amide cases listed. The H-bridge of HO_2•(d) to an amide carbonyl oxygen is a common feature of all amide starting complexes, as well as the extended spin density on the amide(s). As in the case of H-abstraction from N2-β-H by HO_2•(d), the relatively high activation barrier in this case is due to steric hindrance around the tertiary N3 in the transition state.

 doi:10.20944/preprints202501.2059.v1

In short, HO_2•(d), HO•(d) and α- and β-amino peroxy radicals contribute to propagation in the FCRA of PEI. All activation barriers for propagation are significantly lower than the experimental and computational activation barrier for initiation of FCRA of BPEI, which are 135.0 and 133.2 kJ/mol respectively.

Decomposition of α-amino hydroperoxides and H-abstraction from CH_2-groups of the N,N-3,4-dimethyl N6 pentamer by HO_2•(d) show the highest activation barriers, ranging from 84.1 to115.7 kJ/mol. This computational range coincides very well with the range between 90-110 kJ/mol during propagation experimentally observed by Nezam et al.[10].

H-abstraction from CH_2-groups of the N,N-3,4-dimethyl N6 pentamer amides by HO_2•(d) shows activation barriers, ranging from 70.6 to100.0 kJ/mol and will play a role in a later stage of the oxidation with conversion ≥ 70% particularly.

Propagation by HO•(d) shows much lower activation barriers, ranging from 9.3 to 21.2 kJ/mol only, while propagation by various amino peroxy radicals shows activation barriers, ranging from 32.4 to 80.2 kJ/mol. Both processes contribute to propagation but are mainly limited to a single PEI-oligomer.

With some caution it can be concluded also that the exact geometry of the PEI-oligomer, as has become clear from the PEI-model, N,N-3,4-dimethyl N6 pentamer, can play an important role in propagation reactions, either by stabilizing or destabilizing starting structures and transition states, thus affecting activation barriers. Caution is needed because of the inherent limitations of the PEI-model used, and the notion that PEI-oligomers are extremely flexible with a huge amount of conformers.

4.4. Side Reactions

4.4.1. Propagation with Various α-Amino CH•(d) Radicals and H_2O_2

Thus far propagation reactions have been considered starting from the PEI-model, N,N-3,4-dimethyl N6 pentamer, and a chain carrying radicals like HO_2•(d), HO•(d), or α-amino peroxy radicals. The latter is the product from a barrier free reaction of an α-amino CH•(d) radical with O_2(t). In turn an α-amino CH•(d) radical can be the primary result of an H-abstraction by an internal amino peroxy radical, HO•(d) or HO_2•(d) in the FRCA propagation chain.

The result of H-abstraction from N,N-3,4-dimethyl N6 pentamer by HO_2•(d) is an α-amino CH•(d) radical and H_2O_2. As the H_2O_2 is in close vicinity of the α-amino CH•(d) radical, a direct radical hydroxylation might yield an α-amino CH(OH) compound and HO•(d). The HO•(d) radical further contributes to the FRCA radical chain as discussed earlier. This reaction might also occur with oxidation products like the N1-amide-β-radical and the N1,N2-diamide N1-β-radical. The α-amino CH(OH) compound is a so called half aminal. The fate of half aminals strongly depends on the reaction conditions [48]. The presence of sufficient water favors the formation of an aldehyde and an amine, while in the presence of sufficient amines, imine formation is dominant.

It should be kept in mind that the formation of an aldehyde and an amine implies a chain break in PEI. Under dry conditions, in the presence of amines and temperatures > 100°C the half aminals might either stay partially intact or yield imine structures of the types: RNH-CH_2-C=N-R, RNH-C=O-C=N-R and RNH-C=O-C=N-C=O-R. RNH-CH_2-C=N-R and RNH-C=O-C=N-R were identified as structural units by Ahmadalinezhad and Sayari [13] but RNH-C=O-C=N-C=O-R was not.

However, the reaction with H_2O_2 has to compete with the barrier free reaction with O_2(t). So an estimate has to be made of the relative rates of these parallel reactions, starting from the α-amino CH•(d) radical, the N1-amide-β-radical and the N1,N2-diamide N1-β-radical. As no literature data are available on neither oxygen nor H_2O_2 solubility in PEI-800 at temperatures between 125°C and 150°C, a rough estimate was made, based on the ΔΔH of interaction of O_2(t) and H_2O_2 , and the ΔΔEa of the reaction of O_2(t) and H_2O_2 with an α-amino CH•(d) radical of the N,N-3,4-dimethyl N6 pentamer.

 doi:10.20944/preprints202501.2059.v1

Table 2 shows the results. The interaction enthalpy of O_2 for all complexes is approximately -4.2 kJ/mol and the activation barrier for reaction with O_2(t) is 0.0 kJ/mol. Therefore, these values are not listed in Table 2. Furthermore, the effect of temperature turned out to be relatively small (5-25%) and not a discriminating factor between the two parallel reactions. Therefore, results of calculations at 137.5°C are listed only.

Table 2. Overview B3LYP/6-31G* interaction enthalpies with H_2O_2, activation barriers for hydroxylation by H_2O_2 of various N,N-3,4-dimethyl N6 pentamer radicals, and the resulting estimates for $[H_2O_2]/[O_2]$, k-H_2O_2/k-O_2, and r-H_2O_2/r-O_2 at 137.5°C. All calculations are based on the simple approximation: $\Delta G \sim \Delta H = -RT*\ln K$ and $\Delta E_a \sim \Delta H_a = -RT*\ln k$.

N,N-3,4-dimethyl N6 pentamer radical	DH H_2O_2 (kJ/mol)	E_a H_2O_2 (kJ/mol)	$[H_2O_2]/[O_2]$	k-H_2O_2/k-O_2	r -H_2O_2/r-O_2
N1-a-amino radical	-35.4	37.1	$9.37*10^{3}$	$1.90*10^{-5}$	$1.78*10^{-1}$
N1-amide-b-radical	-59.3	60.8	$1.04*10^{7}$	$1.83*10^{-8}$	$1.89*10^{-1}$
N1,N2-diamide N1-b-radical	-58.2	90.9	$7.40*10^{6}$	$2.70*10^{-12}$	$2.00*10^{-5}$

From Table 2 for the N1-α-amino radical and the N1-amide-β-radical, the overall reaction rate of direct hydroxylation with H_2O_2 is 18-19% of the rate of hydroperoxide formation. It should be kept in mind that apart from the possible error in the calculations, the quantitative result of such a comparison is quite sensitive to the actual levels of O_2(t) and H_2O_2. It is also clear that the absolute value of the H_2O_2 interaction enthalpy should be approximately equal to the H_2O_2 activation barrier as only under these circumstances the product of $[H_2O_2]/[O_2]$ * k-H_2O_2/k-O_2 yields an r -H_2O_2/r-O_2 with a considerable fraction of the overall parallel reaction rate from the hydroxylation by H_2O_2. Figure 7 shows the starting complexes and transition states of the reaction of H_2O_2 with the N1-α-amino radical and the N1-amide-β-radical.

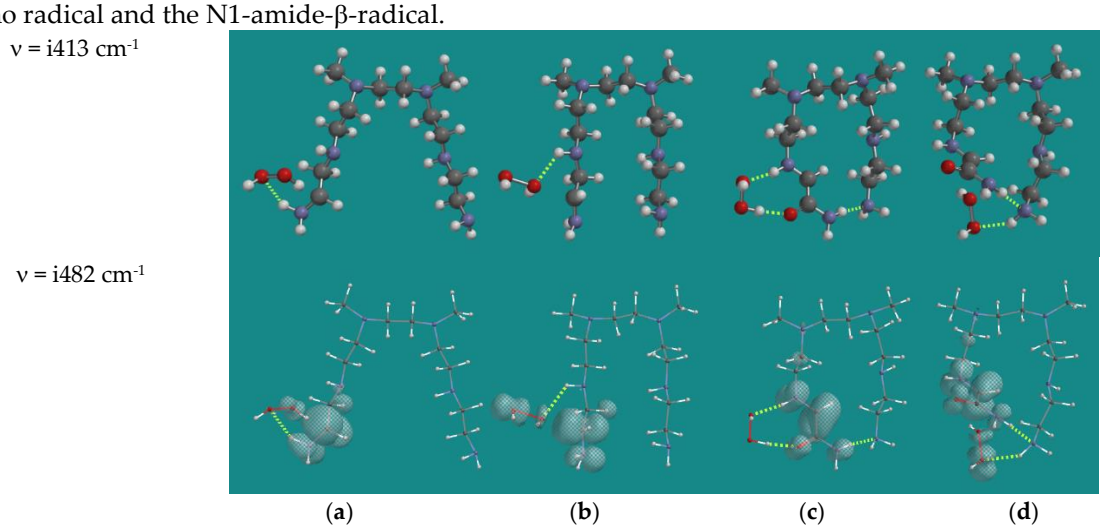

Figure 7. B3LYP/6-31G* starting complexes and transition states of the reaction of H_2O_2 with the N1-α-amino radical and the N1-amide-β-radical of the N,N-3,4-dimethyl N6 pentamer; a: starting complex, and b: transition state of H_2O_2 - N1-α-amino radical, c: starting complex, and d: transition state of H_2O_2 - N1-amide-β-radical. Display upper: ball and spoke, display lower: ball and wire, C: grey, N: blue, H: white, hydrogen bridges: yellow; surface: spin density at isosurface =0.002 e/au^3.

The starting complex (a) of the N1-a-amino radical of the N,N-3,4-dimethyl N6 pentamer is the product complex of the H-abstraction reaction of HO_2•(d) and N1-a-H of the N,N-3,4-dimethyl N6 pentamer, listed in Table 1, entry 16. The -OH still points to the N1-a-amino radical. The OH- CH•(d) distance is 1.942 Å, the O - CH•(d) distance is 2.900 Å. Furthermore, there is a weak H-bridge between the N1- amine group and the OH of H_2O_2 with a distance of 2.588 Å. The resulting lower electron density on the N1-amine has led to the absence of an N1-amine-N6-amine H-bridge. The O-O distance in H_2O_2 is 1.458 Å but the spin density plot shows that there is still some spin density left on

 doi:10.20944/preprints202501.2059.v1

that oxygen. The interaction energy is -35.4 kJ/mol. In the transition state (b) the OH-group of H_2O_2 has rotated out of the way and the O - CH•(d) distance is shortened to 2.333 Å. In addition, a rather weak H-bridge between the N2- amine group and the OH of H_2O_2 is present with a distance of 2.268 Å. The O-O distance in H_2O_2 has increased to1.618 Å. There is spin density on both oxygens of H_2O_2 while the spin density on the N1-a-amino radical seems not to have changed a lot. The imaginary frequency n = i413 cm^{-1} shows C-C bond formation and OH•(d) as leaving group. The activation barrier is 37.1 kJ/mol.

The starting complex (a) of the N1-amide-b-radical of the N,N-3,4-dimethyl N6 pentamer is stabilized by H-bridges to the N1-amide oxygen and the N2-amine with distances of 1.707 Å and 1.945 Å respectively. In addition, there is an H-bridge between the N1- amine group and the N6-amine with a distance of 2.091 Å. The O - CH•(d) distance is 3.875 Å. Spin density is on the N1-amide-b-radical only with the highest spin density on the radical center itself and significant contributions on the N1-amide and the N2-amine. The O-O distance in H_2O_2 is 1.455 Å in line with the absence of spin density. The interaction enthalpy has increased to -59.3 kJ/mol.

In the transition state (b) H_2O_2 has approached the radical center, resulting in an O - CH•(d) distance of 2.307 Å, and the O-O distance in H_2O_2 has increased to1.661 Å, both close to the corresponding distances observed in the first case. In addition, H-bridges between the N1- amide group and the OH of H_2O_2 both with the N6-amine are present with distances of 2.002 Å and 2.307 Å respectively. There is considerable spin density on both oxygens of H_2O_2 while the spin density on the N1-a-amino radical seems not to have changed a lot. The imaginary frequence of n = i413 cm^{-1} shows C-C bond formation and OH•(d) as leaving group. The activation barrier has increased to 60.8 kJ/mol.

The third case, the N1,N2-diamide N1-β-radical, shows a similar stabilization of the starting complex as the starting complex of the N1-amide-β-radical, which leads to an almost equal interaction enthalpy of -58.2 kJ/mol. However, the transition state structure shows a decreased electrostatic charge of 0.023 on the carbon with the highest spin density compared to the transition state structure of the N1-amide-β-radical with an electrostatic charge of -0.193, which results in an increased activation barrier of 90.0 kJ/mol. This makes the direct hydroxylation with H_2O_2 so slow that it will not contribute to propagation and that the corresponding half-aminal will not be observed.

The results can be summarized as follows: air oxidation of PEI-800 leads to the formation of α-amino radicals via H-atom abstraction by O_2(t) or HO_2•(d). In the next oxidation step these α-amino radicals can undergo two parallel reactions: 1) with another O_2(t) to yield α-amino peroxy radicals, or 2) with H_2O_2 formed from HO_2•(d) to yield the corresponding half-aminals. Computational results of these parallel oxidation reactions indicate that reaction with H_2O_2 could contribute considerably to propagation in PEI-800 itself, as mimicked by the N1-α-amino radical of the N,N-3,4-dimethyl N6 pentamer and the partially to amides oxidized analogues. The reaction seems highly unlikely for partially to amides oxidized analogues where the amide groups are next to each other. The products of these two reactions, half-aminals with structural units RNH-CH_2-C(OH)NN-R and RNH-C=O-C(OH)NH-R might partly lose H_2O under dry conditions at temperatures > 125°C to yield RNH-CH_2-C=N-R and RNH-C=O-C=N-R structural units, which were experimentally observed by Ahmadalinezhad and Sayari [13] using advanced NMR-techniques.

4.4.2. β-Elimination of N-β-CH•NHR(d) Radicals

While investigating propagation with α-amino peroxy radicals, a consecutive reaction was identified. In case of a lack of oxygen the product of Table 1 entry 12, the N2-β-amino hydroperoxide-N3-β-CH•NHR(d) radical, can undergo a β-elimination leading to cleavage of C-N3 bond of the tertiary amine to yield two fragments consisting of a secondary amine radical, the N-methyl-N•(d)-ethylene diamine dimer, and the N-methyl, vinyl-ethylene diamine dimer. The activation barrier is 88.3 kJ/mol, close to the value reported of 90 kJ/mol by Racicot et al., [11] for a similar reaction leading to NH_3 . The experimental results of Nezam et al., [10] provides a clue for a lack of oxygen in the case

Preprints.org (www.preprints.org) | NOT PEER-REVIEWED | Posted: 28 January 2025 doi:10.20944/preprints202501.2059.v1

of oxidation with 5% O_2, which shows a weight loss of 17% compared to 12% in case of oxidation with 17 or 30% O_2.

Figure 8 shows the starting structure, the transition state and the product. In the starting structure the spin density is mainly on the N3-β-carbon and N4. This is reflected in the distance between these atoms of 1.394 Å. The distance between N3-α-C and N3-β-C is 1.511 Å. The OH-group of the hydroperoxide and the N3 provide some additional stabilization to the radical. There is no clear N3-HO H-bridge as can be seen from the distance N3-HOOR of 2.541 Å.

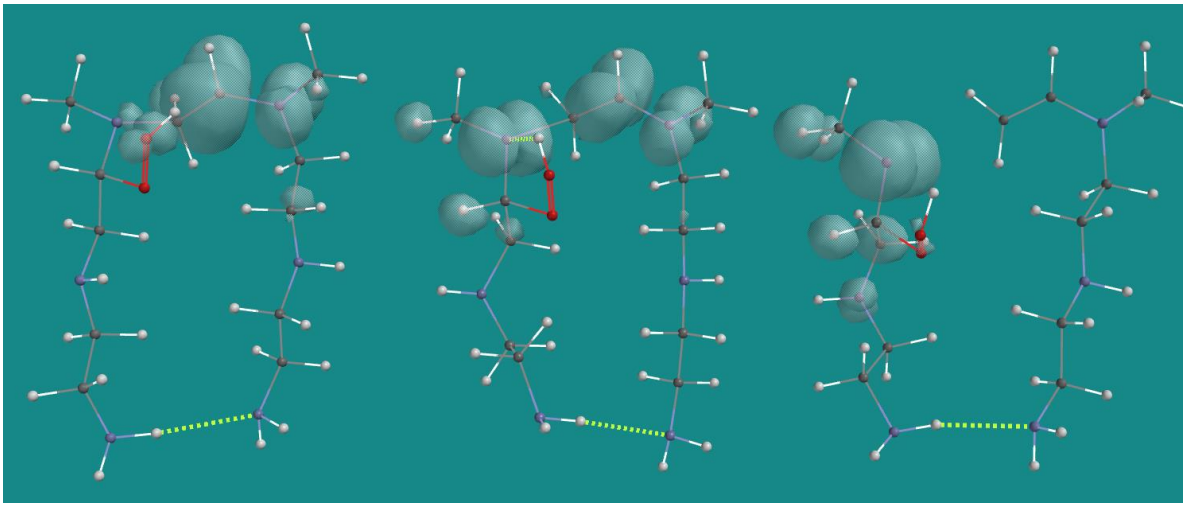

ν = i330 cm^{-1}

(**a**) (**b**) (**c**)

Figure 8. B3LYP/6-31G* β-elimination of N2-β-amino hydroperoxide-N3-β-CH•NHR(d) radical of N,N-3,4-dimethyl N6 pentamer; a: starting complex, b: transition state, c: product complex. Display: ball and wire, C: grey, N: blue, H: white, hydrogen bridges: yellow; surface: spin density at isosurface =0.002 e/au^3.

In the transition state there is still a large spin density on the N3-β-carbon and N4 and the distance between these atoms of 1.368 Å has only changed slightly. The distance between N3-α-C and N3-β-C has shortened to 1.386 Å, a clear sign of the formation of a double bond. There is also a large spin density on the N3-atom, and now there is a clear N3-HO H-bridge with a distance N3-HOOR of 1.910 Å. Apparently a radical on C or N is seriously stabilized by an OH-group in close vicinity as this is visible in the starting structure and the Transition State. The largest change is observed in the distance between N3-a-C and N3-b-C which has enlarged to 2.141 Å, a clear sign of bond breaking.

In the product complex the spin density on the (former) N3-b-carbon and N4 has disappeared and the formation of the double bond has completed. The spin density now is dominant on the N3-atom with residual spin density on the a-C hydrogen atoms. The distance between N3-a-C and (former) N3-b-C has enlarged to 3.767 Å. The reaction thus far is endothermic with ~40 kJ/mol. However the N•-radical is a reactive intermediate which will abstract a H-atom. The most favorable reaction is H-atom abstraction from the H-bridged hydroperoxide to yield the a-amino peroxy radical. This reaction has an activation barrier of 48.5 kJ/mol and an estimated reaction energy of -58.5 kJ/mol. So the overall reaction enthalpy turns from endothermic to slightly exothermic with -19 kJ/mol. The resulting the a-amino peroxy radical will further contribute to the propagation. The visually attractive 1,2-H-shift from C to N, yielding the amide and the HO•(d) radical, has an activation barrier of 164.8 kJ/mol, and it extremely unlikely to occur.

Peroxy radicals can undergo several self-reactions also as described in reaction 3 and 4. These reactions have been investigated computationally in-depth [29,30]. The self-reactions lead to two alkoxy radicals and O_2(t) (propagation reaction 3), a carbonyl and an alcohol compound and O_2(t) (termination reaction 4), or a peroxide and O_2(t). These reactions presume either 2 RO_2•(d) radicals in close vicinity or the formation of a reactive tetroxide intermediate RO_4R. The formation of an intermediate tetroxide turned out to be an equilibrium reaction with a DG ~ 0.0 kJ/mol for R= 2-butyl.

 doi:10.20944/preprints202501.2059.v1

Assuming that the steric demands in the PEI-800 case for two peroxy radicals will be at least similar to the one observed for a single peroxy radical of ~40 kJ/mol, the self-reactions of two α-amino peroxy radicals inside the PEI-800 model seem not very plausible, neither as propagation nor as termination reaction. However, as described by Salo et al., [30] the reaction between a peroxy radical and an HO_2•(d) radical is very possible. The main product of that reaction is the corresponding hydroperoxide and O_2(t) [15,30], but the formation of a small amount of an alkoxy radical, O_2(t) and an HO•(d) radical is possible too as the overall reaction energy is slightly exothermic by -8 kJ/mol and the reaction barriers are very low with values ranging from 0-12 kJ/mol. Alkoxy radicals are very reactive and show H-abstraction and neighboring C-C bond cleavage reactions [27]. Thus, though not of major importance for propagation, H-abstraction and C-C bond cleavage reactions of N1-, N2-, and N3-α-amino oxy radicals of the N,N-3,4-dimethyl N6 pentamer were investigated as they might offer an explanation for some side-products. Table 2 lists an overview of the results.

Table 3. Overview B3LYP/6-31G* activation barriers and reaction enthalpy H-abstraction and reaction enthalpy C-C bond cleavage reactions of N1-, N2-, and N3-α-amino oxy radicals of N,N-3,4-dimethyl N6 pentamer.

N,N-3,4-dimethyl N6 pentamer	n TS	E_a H-abstraction	DH H-abstraction	DH C-C cleavage
	cm^{-1}		kJ/mol	
N1-a-amino oxy radical	i615	-1.9	-39.2	-92.0
N2-a-amino oxy radical	i1310	25.3	-22.4	-116.2
N2-b-amino oxy radical	i325	0.9	-36.6	-113.1

Activation barriers of the C-C bond cleavage reactions are not listed as they could not be determined. Though semi-empirical PM3 calculations yielded transition states for the various C-C bond cleavage reactions with unique imaginary frequencies which upon animation clearly show the desired reaction, B3LYP/6-31G* calculations did not. Starting from PM3 transition state structures, the imaginary frequency was lost in less than 10 optimization steps. An alternative approach, creating an Energy Profile, starting from α-amino oxy radicals and increasing the C-C distance to 2.5 Å in steps of 0.1 Å, resulted in a continuous descending total energy curve as function of the increasing distance. With some caution it can be concluded that the C-C bond cleavage reactions are barrier free.

The activation barriers for H-abstraction for the N1-α-amino oxy radical and the N2-β-amino oxy radical are close to 0 kJ/mol. With respect to the negative activation barrier for H-abstraction of the N1-α-amino oxy radical it should be noted that the B3LYP/6-31G* total energy of the transition state is 7 kJ/mol higher than the total energy of the starting structure but its zero point energy is 9 kJ/mol lower, resulting in an activation barrier of -1.9 kJ/mol. The activation barrier for H-abstraction for the N2-α-amino oxy radical with 25.3 kJ/mol is significantly higher than the N1 and N2 cases. This is due to steric hindrance in the transition state albeit not that much as in the case of the H-abstraction of the N2-α-amino peroxy (d) radical (Table 1, entry 11). Figure 9 shows an overview of the H-abstraction reaction for the N2-α-amino oxy radical.

 doi:10.20944/preprints202501.2059.v1

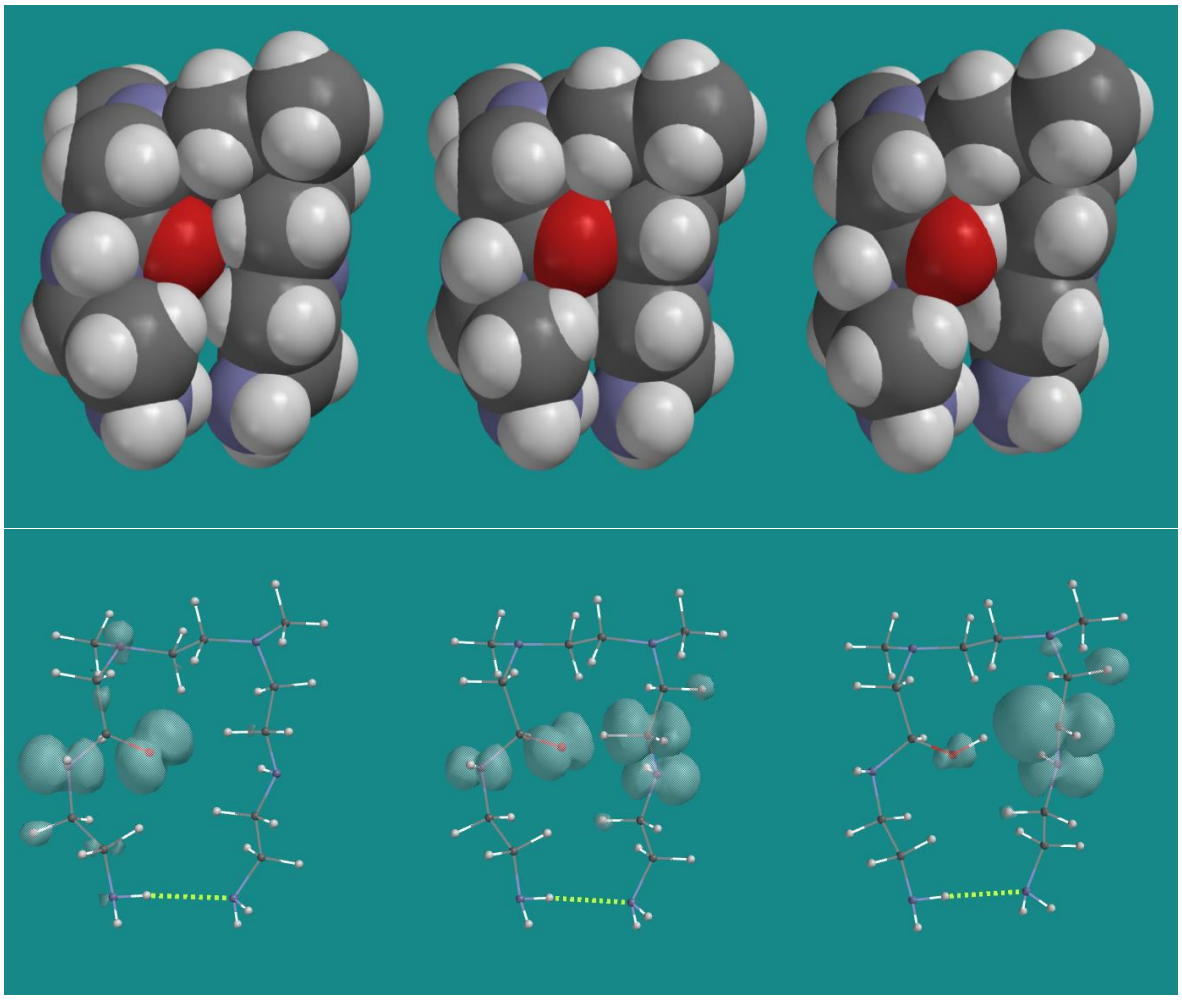

ν = i330 cm^{-1}

(**a**) (**b**) (**c**)

Figure 9. N4 β-H-abstraction of the N2-α-amino oxy radical of N,N-3,4-dimethyl N6 pentamer; B3LYP/6-31G*. a: starting complex, b: transition state, c: product complex. Display upper: space filling; display lower: ball and wire, C: grey, N: blue, H: white, hydrogen bridges: yellow; surface: spin density at isosurface =0.002 e/au^3.

The space filling display gives a clear indication of steric hindrance in all three situations, but it is apparently highest in the transition state. In the product the steric hindrance still accounts for approximately 14-17 kJ/mol as can be deducted from the difference from the ΔH H-abstraction by the N2-α-amino oxy radical compared with the ΔH H-abstraction by the N2-α-amino oxy radical and the N2-β-amino oxy radical.

Primary products of these H-abstraction reactions are again half-aminals and a-amino CH•(d) radicals. The radicals in turn will react with oxygen or H_2O_2 as discussed before and could deliver a limited contribution to propagation.

4.4.3. Formation of NH_3.

In case of a half aminal originating from a primary amine, one of the products will be NH_3. This reaction thus provides an explanation for the formation of NH_3 from primary amines in PEI-800.

According to Hermans et al., [27] in the FRCA of cyclohexane the alkoxy radical yields ~60% cyclohexanol and ~40% of ω-formyl product, based on the minor differences in activation barriers between the two reactions. In the PEI-800 case the activation barriers of both reactions are ~0 kJ/mol, resulting in a 50% contribution for each of them. Thus, the maximum amount of NH_3 formation from initial primary amines should be ~20% because the amount of primary amines in PEI-800 is ~40% as described below Figure 1. Racicot et al. [11] reported an NH_3 production of 21% (mmol NH_3/mmol PEI-800). So, the computational results coincide well with the experimental ones. Finally, if NH_3 is

 doi:10.20944/preprints202501.2059.v1

produced from a half-aminal, the other product should be an aldehyde. However, in an environment with a high amount of amines, the aldehyde will be converted rapidly to an imine and H_2O.

4.4.4. Formation of CO_2.

Products of the C-C bond cleavage reactions of α-amino oxy radicals of the N,N-3,4-dimethyl N6 pentamer are N-formamides and $R_1R_2NCH_2$•(d) radicals. The $R_1R_2NCH_2$•(d) radicals will react barrier free with oxygen to yield The $R_1R_2NCH_2O_2$•(d) peroxy radicals, which eventually will yield N-formamides too via the corresponding hydroperoxides as discussed earlier. Air oxidation of various formamides with the HO•(d) radical as initiator has been studied experimentally and computationally by Bunkan et al., [49] in their research on atmospheric chemistry. In the gas phase H-abstraction by the HO•(d) radical from the aldehyde of N-methyl formamide is the main reaction with a yield of 83%. The consecutive reaction with O_2 leads to methyl isocyanate (78%) by H-abstraction from nitrogen, and the N-CH_3 amide peroxy radical (22%). Isocyanates could react easily with amines to yield urea compounds. Urea compounds are well known as the products from deactivation of amine resins by CO_2 [50] but not by O_2(t). Related to atmospheric chemistry also, a computational study to the reaction of the HO_2•(d) radical with acetaldehyde [51] established that the HO_2•(d) radical reacts easily with acetaldehyde to yield the corresponding the α-hydroxyethyl peroxy radical. The authors pointed out that the HO_2•(d) radical is present in much higher concentration than the HO•(d) radical. Therefore, in FRCA of PEI it seems more obvious to study the reaction of a formamide with HO_2•(d) than the reaction between formamide and HO•(d). Formamide and N-methyl formamide were taken as small model system for PEI. As all computational results obtained were similar for both systems, the results of formamide and N-methyl formamide will be discussed simultaneously.

Direct H-abstraction from formamide and N-methyl formamide by HO_2•(d) yields the N-acyl radical and H_2O_2 with an activation barrier of 97.2 and 94.2 kJ/mol respectively. A visual attractive consecutive reaction would be the direct formation of the carbamic acid and HO•(d). However the initial H-abstraction by HO_2•(d) is endothermic by 84.9 and 83.5 kJ/mol respectively and upon the desired approach of H_2O_2 to the N-acyl radical, the reverse reaction shows activation barriers of 12.3 and 10.7 kJ/mol only. Furthermore, no transition state for the formation of the carbamic acid and HO•(d) could be determined.

By creating an Energy Profile of the approach of HO_2•(d) to formamide or N-methyl formamide an energy maximum was observed with a C-O distance of ~2.0 Å and an OOH-O=C distance of ~1.4 Å, indicating an HO_2•(d) addition to the carbonyl function. Transition States could be established in both cases with activation barriers of 50.5 and 51.5 kJ/mol for formamide and N-methyl formamide respectively. Figure 10 shows the starting structure, transition state and product structure for N-methyl formamide.

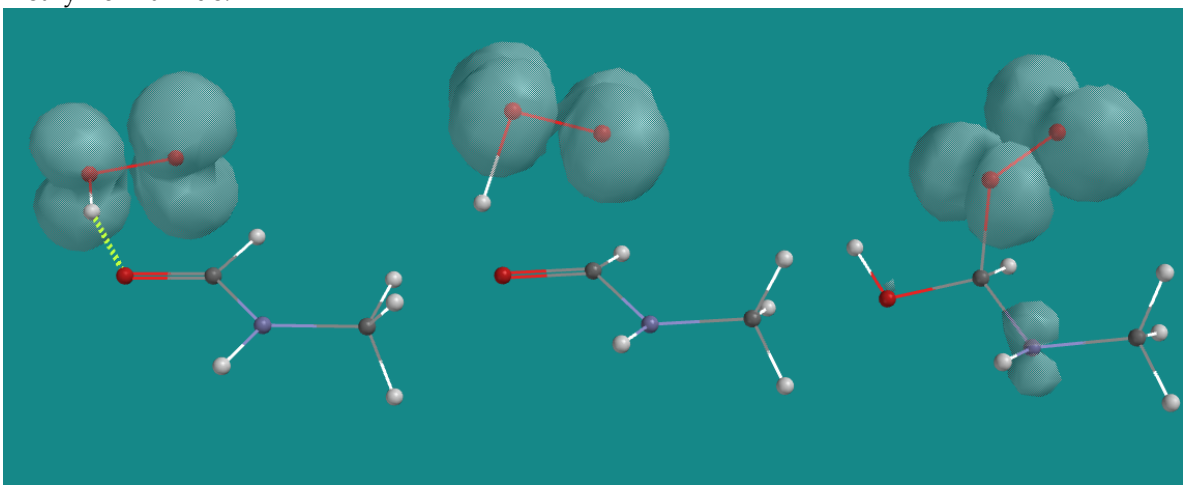

ν = i337 cm^{-1}

(**a**) (**b**) (**c**)

 doi:10.20944/preprints202501.2059.v1

Figure 10. Addition of HO_2•(d) to N-methyl formamide; B3LYP/6-31G*. a: starting complex, b: transition state, c: product complex. Display: ball and wire, C: grey, N: blue, H: white, hydrogen bridges: yellow; surface: spin density at isosurface =0.002 e/au^3.

In the transition state the OH distance is 1.087 Å and the O-C distance is 2.024 Å, indicative for process where proton transfer precedes O-C bond formation. The radical character remains on the O-O part as can be seen from the spin densities in all three structures.

In the second step H-transfer takes place with another HO_2•(d) yielding the hydroperoxide and O_2(t). This is the usual type of low barrier H-atom transfer with an activation barrier of 10.2 and 8.4 kJ/mol for formamide and N-methyl formamide, respectively.

The third step is CH H-abstraction from the hydroperoxide by HO_2•(d), yielding the carbamic acid derivatives of formamide and N-methyl formamide, H_2O_2 and the HO•(d) radical with activation barriers of 57.2 and 59.8 kJ/mol respectively. The HO•(d) thus formed reacts barrier with H_2O_2 to yield H_2O and HO_2•(d).The activation barrier is 4.6 kJ/mol only. The carbamic acids might lose CO_2 easily via amine catalysis.

Keeping in mind that the reaction between an N-α-amino peroxy radical of N,N-3,4-dimethyl N6 pentamer and an HO_2•(d) radical to yield an N-α-amino oxy radical of N,N-3,4-dimethyl N6 pentamer is a side-reaction, the overall sequence of reactions provides a plausible explanation for the formation of a limited amount of CO_2, consistently using HO_2•(d) as the chain carrying radical.

5. Discussion

5.1. Set of Propagation Reactions

The oxidation of PEI is described best as a BAS process or FRCA [25,26) with Initiation, Propagation and Termination as important conceptual steps. Decomposition of the initially formed α-amino hydroperoxide is the first step in Propagation. Propagation occurs partly via α-amino CH•(d) radicals, peroxy radicals, OH-radicals inside an PEI oligomer, and mainly via HO_2 radicals both inside and between different PEI oligomers.

All computational findings are supported by earlier experimental findings with respect to activation barriers, structural elements identified in the oxidized PEI, and volatile products like NH_3, H_2O and CO_2. Additional support for various steps was found in the literature on FRCA processes like the oxidation of cyclohexane and toluene.

A specific role in the propagation plays the reaction of various α-amino CH•(d) radicals of PEI with H_2O_2. Direct hydroxylation with H_2O_2 accounts for approximately 16% of the overall propagation. The product of that reaction is a half aminal RNH-C(OH)CH_2NR_2 which in case of a primary amine under dry conditions and T> 125°C leads to the formation of NH_3 and an imine, and in case of secondary or tertiary amine, to chain breaks and imine formation.

The computational result for NH_3 formation quantitatively coincides with the experimental one of approximately 20%. In addition, it provides an explanation for the small amount of CO_2 experimentally observed, via the oxidation of N-formamide species with HO_2(d). The N-formamide species are the product of the direct hydroxylation with H_2O_2, or the H-abstraction reaction of alkoxy radicals, in both cases eventually leading to half aminals.

Thus a simplified overall scheme for propagation in FRCA of PEI can be set up:

20) PEI-α-amino CH-OOH + HO_2•(d) → PEI-amide + HO_2•(d)

21) PEI + HO_2•(d) → PEI-α-amino CH(d) + H_2O_2

22) PEI-a-amino CH(d) → O_2(t) → PEI-a-amino CHO_2•(d)

22) PEI-a-amino CH(d) → H_2O_2 → PEI-a-amino CHOH + HO_2•(d)

23) PEI-α-amino CHO_2•(d) + PEI → PEI-α-amino CH-OOH + PEI-α-amino CH(d)

 doi:10.20944/preprints202501.2059.v1

In this simplified scheme with five reactions only it is important to note that is assumed that HO•(d) in most cases will react barrier free and very fast with either H_2O_2 or HO_2•(d) to yield H_2O and HO_2•(d) or O_2(t) as H_2O_2 and HO_2•(d) are present in close vicinity. Additionally, H-abstraction of PEI by HO•(d) could occur to yield H_2O and PEI-α-amino CH(d).

The activation barriers for the H-abstraction from PEI-α-amino CH-OOH and PEI itself by HO_2•(d) range from 84.1-115.7 kJ/mol, or approximately 100 kJ/mol on average, in line with the experimental findings from Nezam et al., [10] of 105 ± 10 kJ/mol for the overall activation barrier of FRCA of PEI up to 60% conversion, and in line with the observation that loss of amine efficiency precedes heat production.

The reaction of PEI-α-amino CH(d) with O_2(t) is barrier free. The reaction of PEI-α-amino CH(d) with H_2O_2 shows an activation barrier of 37.1 kJ/mol, while the analogue reaction of an N-amide-β-radical shows an activation barrier of 60.8 kJ/mol. Finally, the reaction of PEI-α-amino CHO_2•(d) with PEI shows activation barriers ranging from 32.4-80.2 kJ/mol.

It can be concluded that up to a conversion of approximately 60%, FCRA of PEI is dominated by H-abstraction from PEI-α-amino CH-OOH by HO_2•(d) and that thereafter H-abstraction from PEI and PEI-amides by HO_2•(d) takes over slowly with slightly lower average activation barriers.

5.2. Final Products of FRCA of PEI

Thus far the focus was entirely on possible reactions contributing to propagation in FCRA of PEI. Experimentally determined volatile products like NH_3, H_2O and CO_2, and elucidated structural elements in the final product, like amides, and several types of imines were used to establish the plausibility of the reactions computationally investigated. In this section an attempt will be made to describe the final product of FRCA of PEI, described by Nezam et al., [10].

They found that the fully oxidized PEI-800, still contains 3.5 H per repeat unit, compared to 5 H per repeat unit in pristine PEI, and that the chain length of PEI has dropped from 19 to 15. The mass retained after complete oxidation is approximately 87% as a net result of mass increase, due to the incorporation of oxygen, and mass loss, due to the production of NH_3, H_2O and CO_2. The amount of NH_3 produced was 0.2 mol/mol repeat units in PEI, corresponding to approximately 50% of the primary amines in pristine PEI and the corresponding C/N ratio. The amount of H_2O produced was 0.5 mol/mol repeat unit in PEI while the CO_2 production is very low with ~0.01 mol/mol repeat unit [10,11]. All experimental data were combined and put in Table 4 to get an idea what the fully oxidized PEI oligomer looks like, and what the contribution of the different reactions identified is to the final product.

Table 4. Composition of the various structural elements in a fully oxidized PEI-800 oligomer combined with values obtained from elemental analysis, volatile products measured, and mass retained.

Name	PEI unit	Mw	H/(C+N)	N/C	n	c-H/(C+N)	c-N/C	c-Mw
		g/mol						g/mol
pristine	CH_2CH_2NH	43	1.67	0.50	**1.5**	2.50	0.75	64.5
amide	C=O-CH_2NH	57	1.00	0.50	**6.0**	6.00	3.00	342.0
half aminal	CH(OH)-CH_2NH	59	1.67	0.50	**2.0**	3.33	1.00	118.0
imine	CH_2CH=N	41	1.00	0.50	**1.5**	1.50	0.75	61.5
imine-NH_3	CH_2CH	27	1.50	0.00	**3.0**	4.50	0.00	81.0
imine-amide	C=O-CH=N	55	0.33	0.50	**1.0**	0.33	0.50	55.0
Sum					**15.0**	**1.21**	**0.40**	**722.0**
Exp. values					**15.0**	**1.25-1.50**	**0.42-0.43**	**725.6**

The left side of Table 4 contains input data. It starts with trivial names for structural PEI repeat units, which are specified in the next column with a formula description. The third column contains the molecular weight of these units. The fourth and fifth columns contain their corresponding

 doi:10.20944/preprints202501.2059.v1

absolute H/(C+N) and N/C ratios. The N/C ratio is the inverse of the C/N ratio as reported by Racicot et al., [11]. This is done to avoid division by zero in case of the entry imine-NH_3, representing the case of NH_3 loss from primary amines. The middle column contains the number (n) of the various structural PEI repeat units, contributing to the fully oxidized PEI-800 oligomer. It sums up to 15, as experimentally obtained [10]. The columns to the right side of the table contain calculated ratios c-H/(C+N), c-N/C and c-Mw, for all structural PEI repeat units. The last two rows, Sum, and Experimental values (Exp. Values) contain the sum of the various structural PEI repeat units (n), the weighted sum of the calculated ratios c-H/(C+N), c-N/C. and the calculated molecular weight of the fully oxidized PEI-800 oligomer. The experimental values for H/(C+N) and N/C vary slightly with temperature and oxygen concentration.

The molecular weight of the pristine PEI-800 oligomer is 834 g/mol as shown in, and described below Figure 1. According to Nezam et al., [10], 83% of the mass is retained in fully oxidized PEI-800 at 5% O_2 and 87% at 17 and 30% O_2. The latter value was taken as a reference and thus the mass of a fully oxidized PEI-800 oligomer is: 834 g/mol*0.87 = 725.6 g/mol, listed in the row Experimental value. From the comparison of the calculated values with the experimentally observed values in the last three columns it can be seen that they agree reasonably well.

The purpose of Table 4 was not to obtain a perfect fit with all experimental values but to get a general impression of the composition of the fully oxidized PEI-800 and compare that with the computational values for the activation barriers of the reactions described, leading to the various structural PEI repeat units. Therefore, the resolution of n was limited to a 0.5 unit.

Surprisingly not all CH_2 groups are oxidized in the fully oxidized PEI-800 oligomer, and probably even more surprising is the fact that not even one single CH_2 group in all repeat units is oxidized. Pristine PEI contains 5 H atoms per repeat unit. Fully oxidized PEI still contains ~3.5 H atoms per repeat unit. A direct consequence of this experimental finding is that the FRCA of PEI-800 does not lead to 100% of amide repeat units, as the amide still contains 3.0 H per repeat unit. From Table 4 it becomes plausible that even pristine PEI repeat units should be present, in order to arrive at the overall composition in line with all experimental values. Pristine PEI and half aminal PEI repeat units both contain 5 H atoms per unit, but increasing the contribution of the half aminal at the cost of pristine PEI increases the molecular weight substantially to 746 g/mol, corresponding to 90% mass retained, which is not in line with the experimental findings. So it seems that ~10% of pristine PEI repeat units are not oxidized under these conditions. There is no easy explanation for this, but a plausible explanation could be steric hindrance inside PEI-800 oligomers which prevents propagation by HO_2•(d) for specific geometries.

The total amount of α-amino hydroperoxide decomposition leads to ~ 47% of amide products, built up from 6 amide repeat units and 1 amide-imine unit on a total of 15 repeat units. The total amount of direct hydroxylation of α-amino PEI radicals by H_2O_2 in the propagation accounts for ~60%, built up from 3.5 half aminals units, 1.5 imine units, 3.0 imine-NH_3 units, and 1.0 imine-amide units on a total of 15 repeat units.

At first glance this seems significantly larger than the 15% estimate calculated under 4.4.1. Propagation with various α-amino CH•(d) radicals and H_2O_2. However, the assumption that the reaction of the α-amino CH•(d) radicals with O_2(t) has an average activation barrier of 5 kJ/mol leads to a contribution of ~80% to propagation. This does not disqualify the computational results obtained but gives an impression of the sensitivity of the systems. The loss of 3.0 imine-NH_3 units corresponds to an ~16% loss of all amine groups, more precisely NH_3, in line with the experimental findings and the computational result of ~20%. However, the experimentally observed CO_2 production is too low to account for the rest amount of mass loss. The same is true for the experimentally observed loss of H_2O. A plausible explanation for both observations could be that they are stored as various secondary and tertiary ammonium bicarbonates.

There is a rather small variation in the retained mass on full oxidation of PEI-800 as a function of the oxygen concentration. At 5% of O_2, the retained mass is ~83% while at 17 and 30% O_2, the retained mass is ~87%. An obvious way to explain the difference between these values is that at 5%

 doi:10.20944/preprints202501.2059.v1

O_2 less oxygen is incorporated than at 17 and 30% O_2. This might be considered as a sign that some oxygen mass transfer limitation occurs at 5%, however this seems not the case with 17 and 30% O_2. With some caution it can be concluded that oxygen mass transfer limitation was not dominant at the experimental conditions applied, which in itself is in line with a reaction order for O_2 of ~0.5-0.7 [10], and the analysis of Hoorn et al., [33] regarding toluene oxidation under industrial conditions at similar temperatures, that FRCA of toluene is a slow chemical reaction compared to physical mass transfer of oxygen.

Most of the experimental and computational work applies to BPEI, however the experimental work of Ahmadalinezhad and Sayari [13] provides information on LPEI too. The major difference was the absence of imine-amide PEI repeat units which are easily explained by the almost absence of primary amines in LPEI compared to BPEI.

6. Conclusions

In this article a computational study was conducted to Propagation in FRCA of (B)PEI. The study was calibrated using experimental data on air oxidation of BPEI itself and well-known large scale industrial oxidation processes like cyclohexane and toluene oxidation. In addition, literature results of computational studies on cyclohexane and toluene oxidation were used also.

From the computational on the propagation in FRCA of PEI it can be concluded that:

1. The initial formation of α-amino hydroperoxides provides a good explanation for the experimental finding that loss of CO_2 efficiency precedes major heat production in the FCRA of PEI.

2. α-H atom abstraction from α-amino hydroperoxides of PEI by HO_2•(d) is a crucial step in the propagation which yields corresponding amide PEI repeat units, H_2O_2 and OH•(d).

3. The very reactive OH•(d) reacts almost barrier free with H_2O_2 and HO_2•(d) to yield HO_2•(d) and O_2(t) respectively but still might play a limited role in propagation inside a PEI-oligomer.

4. HO_2•(d) is the most important chain carrying radical in the propagation as it not only can react inside a PEI-oligomer but also can transfer the radical chain to other PEI-oligomers.

5. The reaction of HO_2•(d) with a PEI-oligomer leads to a PEI-α-amino CH(d) radical and H_2O_2.

6. The PEI-α-amino CH(d) radical reacts with O_2(t) in a barrier free process to yield the PEI-α-amino peroxy radical, which in turn abstracts an α-H-atom inside a PEI-oligomer in a process to yield PEI-α-amino hydroperoxides with moderate activation barriers. Next the PEI-α-amino hydroperoxides react with HO_2•(d) to yield the corresponding amides as described in conclusion 2. This is a well-known sequence in propagation.

7. In a parallel propagation step the PEI-α-amino CH(d) radicals react directly with H_2O_2 to yield half aminals with the general structure: PEI-α-amino CH(OH).

8. The relative contribution of both reactions to propagation is about 50% for each of them, as calculated from the total amount of amide and imine derived PEI repeat elements.

9. The half aminals with structure PEI primary amine α-amino CH(OH) are the main source for the formation of NH_3 and the computational results provide a quantitative explanation for the amount of NH_3 produced.

10. Half aminals are also the source of various imine structures, identified with advanced NMR techniques.

11. The results of elemental analysis strongly suggest that not all pristine PEI repeat units are oxidized and that approximately 10% remains unaffected. Computational results suggest steric hindrance inside a PEI-oligomer as a possible explanation.

12. Combination of experimental and computational results lead to a semi-quantitative account of the structure of the fully oxidized PEI and the NH_3 produced, but not for the corresponding amounts of H_2O and CO_2. A plausible explanation for this discrepancy is the formation of non-volatile secondary and tertiary ammonium bicarbonate species.

Supplementary Materials: The following supporting information can be downloaded at the website of this paper posted on Preprints.org. Molecular structures (.mol2) (ZIP), Propagation (.xslx), Guidance Supplementary Materials (PDF)

Funding: This research received no funding.

Data Availability Statement: All data are contained in the article and Supplementary Materials.

References

1. D' Alessandro, D. M.; Smit, B.; Long, J. R. Carbon dioxide capture: prospects for new materials. *Angew. Chem., Int. Ed.* 2010, *49*, 6058−6082. DOI: 10.1002/anie.201000431
2. Haszeldine, R. S. Carbon capture and storage: how green can black be? *Science* 2009, *325*, 1647−1652. DOI: 10.1126/science.1172246
3. EPA United States Environmental Protection Agency. U.S. Carbon Dioxide Emissions, 2020. https://www.epa.gov/ghgemissions/overview-greenhouse-gases Date of (access on November 16, 2024).
4. Choi, S.; Drese, J. H.; Jones, C. W. Adsorbent Materials for Carbon Dioxide Capture from Large Anthropogenic Point Sources. *ChemSusChem* 2009, 2, 796−854. DOI: 10.1002/cssc.200900036
5. Goeppert, A.; Zhang, H.; Czaun, M.; May, R. B.; Prakash, G. K. S.; Olah, G. A.; Narayanan, R. R. Easily Regenerable Solid Adsorbents Based on Polyamines for Carbon Dioxide Capture from the Air. *ChemSusChem* 2014, 7, 1386−1397. DOI: 10.1002/cssc.201301114
6. Sanz-Pérez, E. S.; Murdock, C. R.; Didas, S. A.; Jones, C. W. Direct Capture of CO_2 from Ambient Air. *Chem. Rev.* 2016, 116,11840−11876.
7. Shen, X.; Du, H.; Mullins, R. H.; Kommalapati, R. R. Polyethylenimine Applications in Carbon Dioxide Capture and Separation: From Theoretical Study to Experimental Work. *Energy Technol* 2017, 5, 822−833.
8. Veneman, R.; Zhao, W.; Li, Z.; Cai, N.; Brilman, D. W. F. Adsorption of CO_2 and H_2O on supported amine sorbents. *Energy Procedia* 2014, 63, 2336−2345.
9. Alesi, W. R., Jr; Kitchin, J. R. Evaluation of a primary amine functionalized ion-exchange resin for CO_2 capture. *Ind. Eng. Chem. Res.* 2012, 51, 6907−6915.
10. Nezam, I.; Xie, J.; Golub, K. W.; Carneiro, J.; Olsen, K.; Ping, E. W.; Jones, C. W.; Sakwa-Novak, M. A. Chemical Kinetics of the Autoxidation of Poly(ethylenimine) in CO_2 Sorbents. *ACS Sustainable Chem. Eng.* 2021, 9, 8477−8486. https://doi.org/10.1021/acssuschemeng.1c01367
11. Racicot, J.; Li, S.; Clabaugh, A.; Hertz, C.; Akhade, S. A.; Ping, E. W.; Pang, S. H.; Sakwa-Novak, M. A. Volatile Products of the Autoxidation of Poly(ethylenimine) in CO_2 Sorbents. *J. Phys. Chem. C* 2022, 126, 8807−8816.
12. Rosu, C.; Pang, S. H.; Sujan, A. R.; Sakwa-Novak, M. A.; Ping, E. W.; Jones, C. W. Effect of Extended Aging and Oxidation on Linear Poly(propylenimine)-Mesoporous Silica Composites for CO_2 Capture from Simulated Air and Flue Gas Streams. *ACS Appl. Mater. Interfaces* 2020, 12, 38085−38097.
13. Ahmadalinezhad, A.; Sayari, A. Oxidative degradation of silica supported polyethylenimine for CO_2 adsorption: insights into the nature of deactivated species. *Phys.Chem.Chem.Phys*. 2014, 16, 1529.
14. Min, K.; Choi, W.; Kim, C.; Choi, M. Oxidation-stable amine containing adsorbents for carbon dioxide capture. *NATURE COMMUNICATIONS* 2018, 9, 726.
15. Buijs, W. CO_2 Capture with PEI: A Molecular Modeling Study of the Ultimate Oxidation Stability of LPEI and BPEI *ACS Engineering Au* **2023** *3* (1), 28-36. https://doi.org/10.1021/acsengineeringau.2c00033
16. Buijs, W. Role of Fe Complexes as Initiators in the Oxidative Degradation of Amine Resins for CO_2 Capture: Molecular Modeling and Experimental Results Compared *ACS Engineering Au* **2024** *4* (1), 112-124 https://doi.org/10.1021/acsengineeringau.3c00042
17. Chatani, Y.; Tadokoro, H.; Saegusa, T.; Ikeda, H. Structural Studies of Poly(ethylenimine). 1. Structures of Two Hydrates of Poly(ethylenimine): Sesquihydrate and Dihydrate. *Macromolecules* 1981, 14, 315−321.
18. Chatani, Y.; Kobatake, T.; Tadokoro, H.; Tanaka, R. Structural Studies of Poly(ethylenimine). 2. Double-Stranded Helical Chains in the Anhydrate. *Macromolecules* 1982, 15, 170−176.
19. Chatani, Y.; Kobatake, T.; Tadokoro, H. Structural Studies of Poly(ethylenimine). 3. Structural Characterization of Anhydrous and Hydrous States and Crystal Structure of the Hemihydrate. *Macromolecules 1983*, 16, 199−204.

20. Hashida, T.; Tashiro, K.; Aoshima, S.; Inaki, Y. Structural Investigation on Water-Induced Phase Transitions of Poly(ethyleneimine). 1. Time-Resolved Infrared Spectral Measurements in the Hydration Process. *Macromolecules* 2002, 35, 4330−4336.
21. Hashida, T.; Tashiro, K.; Inaki, Y. Structural Investigation of Water-Induced Phase Transitions of Poly(ethylene imine). III. The Thermal Behavior of Hydrates and the Construction of a Phase Diagram. *J. Polym. Sci.*, Part B: Polym. Phys. 2003, 41, 2937−2948.
22. Hashida, T.; Tashiro, K. Structural Study on Water-induced Phase Transitions of Poly(ethylene imine) as Viewed from the Simultaneous Measurements of Wide-Angle X-ray Diffractions and DSC Thermograms. *Macromol. Symp.* 2006, 242, 262−267.
23. Polyethylenimine, branched; product number 408719 https://www.sigmaaldrich.com/AT/de/substance/polyethyleniminebranched1234525987068?utm_source=google&utm_medium=cpc&utm_campaign=9419398930&utm_content=98056962600&gclid=CjwKCAjwjsi4BhB5EiwAFAL0YG6XEh8JeeAkfqel2YUFCyT_DJbGMS7B9r_6vT4lgpPy-rYSyQBIDRoCM4wQAvD_BwE
24. Epomin-SP-012 https://www.shokubai.co.jp/en/products/detail/epomin1/
25. Sheldon, R. A., Kochi, J. Metal-Catalyzed Oxidation of Organic Compounds. Academic Press, Inc.: New York, 1981, 18-24. https://doi.org/10.1021/acs.accounts.8b00250
26. Smith, L. M.; Aitken, H. M.; Coote, M. L. The Fate of the Peroxyl Radical in Autoxidation: How Does Polymer Degradation Really Occur? Acc. Chem. Res. *2018*, 51 (9), 2006−2013
27. Hermans, I., Nguyen, T.L., Jacobs, P.A., Peeters, J. Autoxidation of Cyclohexane: Conventional Views Challenged by Theory and Experiment. *ChemPhysChem* 2005, 6, 637 – 645 DOI: 10.1002/cphc.200400211
28. Hermans, I., Pierre A. Jacobs, P.A., Peeters, J. To the Core of Autocatalysis in Cyclohexane Autoxidation. *Chem. Eur. J*. 2006, 12, 4229 – 4240 DOI: 10.1002/chem.200600189
29. Hasan, G., Valiev, R., Salo, V-T., Kurtén, T. Accretion Products in the OH- and NO_3-Initiated Oxidation of α-Pinene. *J. Phys. Chem. A* 2021, 125, 10632−10639 https://doi.org/10.1021/acs.jpca.1c08969
30. Salo, V-T., Rashid Valiev, R., Lehtola, S., Theo Kurtén, T. Gas-Phase Peroxyl Radical Recombination Reactions: A Computational Study of Formation and Decomposition of Tetroxides. *J. Phys. Chem. A* 2022, 126, 4046−4056 https://doi.org/10.1021/acs.jpca.2c01321
31. Franz, G., Sheldon, R. A. Oxidation. Ullmann's Encyclopedia of Industrial Chemistry, Wiley-VCH, Weinheim, *2012*, 25, 543
32. Hermans, I., Peeters, J., Vereecken, L., Jacobs, P. A. Mechanism of Thermal Toluene Autoxidation ChemPhysChem *2007*, 8, 2678 – 2688 DOI: 10.1002/cphc.200700563
33. Hoorn, J. A. A., van Soolingen, J., Versteeg, G.F. Modelling Toluene Oxidation: Incorporation of Mass Transfer Phenomena. *Chemical Engineering Research and Design*, 2005, 83(A2): 187–195 doi: 10.1205/cherd.04161
34. Spartan '20 and '24 are products of Wavefunction Inc: Irvine, CA, 2021. www.wavefun.com (accessed October 22, 2024).
35. Halgren, T.A. MMFF VII. Characterization of MMFF94, MMFF94s, and other widely available force fields for conformational energies and for intermolecular-interaction energies and geometries *J Comput Chem.* 1999 May;20(7):730-748. doi: 10.1002/(SICI)1096-987X(199905)20:7<730::AID-JCC8>3.0.CO;2-T
36. Grimme,S., Ehrlich, S., Goerigk, L. Effect of the damping function in dispersion corrected density functional theory. *J. Comput. Chem. 2011*, 32(7), 1456–65, DOI 10.1002/jcc.21759.
37. Grimme, S., Hansen, A., Brandenburg J.G., Bannwarth, C. Dispersion-corrected mean-field electronic structure methods. *Chem. Rev.* 2016, 116, 5105−5154 DOI: 10.1021/acs.chemrev.5b00533
38. Goerigk, L. How Do DFT-DCP, DFT-NL, and DFT-D3 Compare for the Description of London-Dispersion Effects in Conformers and General Thermochemistry? *Journal of Chemical Theory and Computation* January 27, 2014 Vol 10/Issue 3 https://pubs.acs.org/doi/abs/10.1021/ct500026v
39. Hehre, W. J.; Ditchfield, R.; Radom, L.; Pople, J. A. Molecular Orbital Theory of the Electronic Structure of Organic Compounds. V. Molecular Theory of Bond Separation. *J. Am. Chem. Soc.* 1970, 92, 4796 https://doi.org/10.1021/ja00719a006
40. Fukui, K. A. Formulation of the Reaction Coordinate. *J. Phys. Chem*. 1970, 74, 4161−4163. https://doi.org/10.1021/j100717a029
41. Franck–Rabinowitch solvent cage effect: IUPAC Compendium of Chemical Terminology, 3rd ed. International Union of Pure and Applied Chemistry; 2006. Online version 3.0.1, 2019. https://doi.org/10.1351/goldbook.C00771 (assessed on November 20, 2024)

42. Keading, W.W., Lindblom, R.O., Temple, R.G., Mahon, H.I., Oxidation of toluene and other alkylated aromatic hydrocarbons to benzoic acids and phenols. *Ind Eng Chem Process Des Dev*, 1965, 4, 97–101 https://doi.org/10.1021/i260013a022
43. Introduction for Noveon Kalama Inc. https://www.chemnet.com/United-StatesSuppliers/7652/Noveon-Kalama-Inc-.html (assessed on November 20, 2024)
44. Buijs, W. Molecular Modeling Study to the Relation between Structure of LPEI, Including Water-Induced Phase Transitions and CO_2 Capturing Reactions. Ind. Eng. Chem. Res. *2021*, 60, 11309−11316. https://doi.org/10.1021/acs.iecr.1c00846
45. Said, R. B.; Kolle, J. M.; Essalah, K.; Tangour, B.; Sayari, A. A Unified Approach to CO2-Amine Reaction Mechanisms. ACS Omega *2020*, 5, 26125−26133 https://doi.org/10.1021/acsomega.0c03727
46. Zvyagin, A.V ., Manson, N. B Chapter 10 - Optical and Spin Properties of Nitrogen-Vacancy Color Centers in Diamond Crystals, Nanodiamonds, and Proximity to Surfaces. Ultananocrystalline Diamond (Second Edition) *2012*, 327-354 https://doi.org/10.1016/B978-1-4377-3465-2.00010-4
47. Wilke, C.R., Chang, P. Correlation of diffusion coefficients in dilute solutions. *Aiche Journal*, 1955, 1, 264-270. https://doi.org/10.1002/aic.690010222
48. Godoy-Alcantar, C., Yatsimirsky, A. K., Lehn, J.-M. Structure stability correlations for imine formation in aqueous solution. *J. Phys. Org. Chem.* 2005, 18, 979–985.
49. Bunkan, A.J.C., Hetzler, J., Mikoviny, T., Wisthaler, A., Nielsen, C.J., Olzmann, M. The reactions of N-methylformamide and N,N-dimethylformamide with OH and their photo-oxidation under atmospheric conditions: experimental and theoretical studies Phys. Chem. Chem. Phys., *2015*, 17, 7046-7059 DOI: 10.1039/C4CP05805D
50. Buijs, W. Direct Air Capture of CO_2 with an Amine Resin: A Molecular Modeling Study of the Deactivation Mechanism by CO_2 Ind. Eng. Chem. Res. *2019*, 58, 14705−14708 DOI: 10.1021/acs.iecr.9b02637
51. da Silva, G., Bozzelli, J.W. Role of the α-hydroxyethylperoxy radical in the reactions of acetaldehyde and vinyl alcohol with HO_2 Chem. Phys. Lett. 2009, 483, (1–3), 25-29.